



#### Available online at www.sciencedirect.com

# **ScienceDirect**



Nuclear Physics A 1037 (2023) 122704

www.elsevier.com/locate/nuclphysa

# Electric conductivity of hot pion matter

Joseph Atchison\*, Ralf Rapp

Texas A&M University, United States of America
Received 16 November 2022; accepted 6 June 2023
Available online 12 June 2023

#### Abstract

The determination of transport coefficients plays a central role in characterizing hot and dense nuclear matter. Currently, there are significant discrepancies between various calculations of the electric conductivity of hot hadronic matter. In the present work we calculate the electric conductivity of hot pion matter by extracting it from the electromagnetic spectral function, via its zero energy limit at vanishing 3-momentum, within the Vector Dominance Model (VDM). Since within the VDM the photon couples to the hadronic currents primarily through the  $\rho$  meson, we use hadronic many-body theory to calculate the  $\rho$ -meson's self-energy in hot pion matter, by dressing its pion cloud with thermal  $\pi$ - $\rho$  and  $\pi$ - $\sigma$  loops including vertex corrections to maintain gauge invariance. In particular, we analyze the low-energy transport peak of the spectral function, extract its behavior with temperature and compare to (the results of) existing approaches in the literature.

Published by Elsevier B.V.

Keywords: Conductivity; Hadronic matter; Pion gas

#### 1. Introduction

A central goal of high-energy nuclear physics is to study and characterize hot and dense nuclear matter which can be created in heavy-ion collisions (HICs) over a large range of center-of-mass energies. A common way to characterize the long-wavelength properties of the medium are transport coefficients, which can be used to describe the transport of conserved charges through the fireball in nuclear collisions. One such coefficient is the electric conductivity,  $\sigma_{el}$ ,

E-mail address: jia08a@acu.edu (J. Atchison).

<sup>\*</sup> Corresponding author.

which will be the focus of this paper. In particular, we will take advantage of the close relation of  $\sigma_{el}$  to the thermal dilepton emission rate [1], as both quantities are directly proportional to the electromagnetic spectral function of the strongly interacting medium. On the one hand, this allows to establish connections between the processes that are widely implemented to describe low-mass dilepton and photon radiation observed in experiments at the SPS, RHIC, HADES and the LHC [2–4]. On the other hand, renewed interest in the conductivity has recently been triggered by future plans to access the pertinent transport peak more directly in experiment through very low-mass and low-momentum dileptons, as being envisaged at the Schwer-Ionen Synchrotron (SIS), the Relativistuc Heavy-Ion Collider (RHIC) and the Large Hadron Collider (LHC) [5–7]. Thus far, available calculations of the electric conductivity of hot hadronic matter have utilized various formalisms and yielded results that vary considerably, by up to an order of magnitude or even more [8–18]. In addition, some of the calculations appear to produce a conductivity that is below a conjectured quantum lower bound proposed in Ref. [9]. In this work, we seek to address the above questions by performing a hadronic quantum many-body calculation of the conductivity, albeit constrained to a system of hot pion matter.

The dilepton emission rate is proportional to the imaginary part of the electromagnetic (EM) current-current correlation function, i.e., the EM spectral function,  $\rho_{EM}$ . At the same time, the electric conductivity can be obtained from  $\rho_{\rm EM}$  as its low-energy limit at zero 3momentum [19-21]. Within the vector dominance model (VDM) the EM correlator is proportional to the light vector meson propagators,  $D_V$ , most notably the  $\rho$ -meson's  $(V=\rho)$ . In the vacuum and in a hadronic description, the latter is related to the  $\rho$ 's self-energy ( $\Sigma_{\rho\pi\pi}$ ), which is governed by 2-pion decays. In the medium, the dressing of the  $\rho$ 's pion cloud in a nuclear medium has been widely studied [22-26], and found to give a key contribution to the low-mass dilepton enhancement observed in experiment. The effects of thermal  $\pi\pi$  scattering, generally believed to be less important, have not been studied as widely [27,28]. However, at relatively small temperatures and vanishing baryon chemical potential baryon-antibaryon excitations are suppressed and the effects of the lighter pions dominate. Since at very low dilepton masses one expects large contributions from the hadronic phase in nuclear collisions, and since at RHIC and the LHC the baryon-chemical potential is small (although contributions from thermally excited baryon-antibaryons are not negligible), a reliable calculation of the conductivity of hot hadronic matter is likely to require the inclusion of thermal pions. Toward this end we here calculate  $\rho_{\rm EM}$ at zero 3-momentum for hot pion matter and analyze the emerging conductivity, thereby serving as a first step in adding thermal  $\pi\pi$  scattering to the baryonic effects calculated in previous works [26].

When dressing the pion cloud of the  $\rho$ -meson with medium excitations, *i.e.*, pion self-energies, it is important to preserve EM gauge invariance, which requires the introduction of appropriate vertex corrections [24,26,29]. The construction of these vertex corrections can be guided by Ward identities, which ensure that the resulting  $\rho$ -meson self-energy, and thus the EM correlation function, is 4-dimensionally transverse, which is a necessary condition for gauge invariance. These vertex corrections were constructed, *e.g.*, in Refs. [24,26,29] for the case of nuclear matter and in Refs. [28,30] for hot pion matter. The introduction of vertex corrections becomes even more challenging in the context of the conductivity, as to render it finite, a dressing of *all* in medium propagators with a finite width is required. In the present work,  $\rho_{\rm EM}$  and the electric conductivity will be calculated in hot pion matter both with and without vertex corrections.

This paper is organized as follows: in Sec. 2 we introduce our microscopic model for the  $\rho$ -propagator and self-energy, first in the vacuum with constraints from scattering data, followed by

the general form at finite temperature and a calculation of the conductivity for on-shell thermal pions that allows to recover the kinetic-theory result. In Sec. 3 we calculate the pion self-energy in a thermal pion gas, based on S- and P-wave scattering through sigma and rho resonances, again constrained by vacuum scattering data. Section 4 is dedicated to the construction of vertex corrections required to maintain gauge invariance at finite temperature. In Sec. 5 we discuss our numerical results for the in-medium EM spectral function, with focus on the low-energy transport peak and pertinent conductivity of hot pion matter, with and without vertex corrections, and put our results into the context of existing literature. In Sec. 6 we discuss two further applications, namely a calculation of the charge susceptibility and a test of a current-conservation sum rule. Finally, we summarize and discuss future work in Sec. 7.

#### 2. Hadronic model for the rho meson

In this section we discuss the connection between thermal dilepton rates and the conductivity via the EM spectral function and compute the latter within VDM (Sec. 2.1) based on a hadronic model for the  $\rho$  propagator. We calculate the  $\rho$  self-energy in vacuum (Sec. 2.2) and at finite temperature (Sec. 2.3), followed by a preliminary on-shell calculation of the conductivity to make contact with kinetic theory (Sec. 2.4).

### 2.1. EM spectral function in the vector dominance model

The thermal dilepton emission rate can be expressed through the EM spectral function as [19, 20]:

$$\frac{dR_{l+l-}}{d^4q} = \frac{\alpha_{\rm EM}^2}{2\pi^3 M^2} f^B(q_0, T) \rho_{\rm EM}(M, q, T, \mu_B) , \qquad (1)$$

where  $f^B$  denotes the Bose-Einstein distribution,  $M^2 = q_0^2 - \vec{q}^2$  is the dilepton's invariant mass, and  $\alpha_{\rm EM} = \frac{e^2}{4\pi}$  the fine-structure constant. The spectral function, in turn, is defined via the imaginary part of the EM current-current correlation in the strong-interaction medium,  $\rho_{\rm EM} = -2~{\rm Im}\Pi_{\rm EM}$ , with a polarization average implied as  $\Pi_{\rm EM} \equiv g_{\mu\nu}\Pi_{\rm EM}^{\mu\nu}/3$ . The electric conductivity can be obtained from the spatial components of the spectral function at zero 3-momentum in the low-energy limit [21],

$$\sigma_{\rm el}(T) = (-e^2/6) \lim_{q_0 \to 0} [\rho_{\rm EM}^{ii}(q_0, \vec{q} = 0, T)/q_0 . \tag{2}$$

Note that at finite T, the retarded spectral function goes linearly to zero with energy, and thus the division by  $q_0$  leads to a finite result provided the imaginary part is non-vanishing for small  $q_0$ .

For invariant masses below approximately 1 GeV, the EM correlator is well described by the VDM, represented by the so-called field-current identity between the vector meson fields,  $V^{\mu}$  and the hadronic EM current:

$$j_{\rm EM}^{\mu} = \frac{m_{\rho}^2}{g_{\rho}} \rho^{\mu} + \frac{m_{\omega}^2}{g_{\omega}} \omega^{\mu} + \frac{m_{\phi}^2}{g_{\phi}} \phi^{\mu} , \qquad (3)$$

where the  $g_V$  denote pertinent hadronic couplings. Since  $g_\omega \simeq 3g_\rho$ , the primary contribution arises from the  $\rho$  meson leading to [31]:

$$\operatorname{Im}\Pi_{\mathrm{EM}}^{\mu\nu} \approx \frac{m_{\rho}^{4}}{g_{\rho}^{2}} \operatorname{Im}D_{\rho}^{\mu\nu} . \tag{4}$$

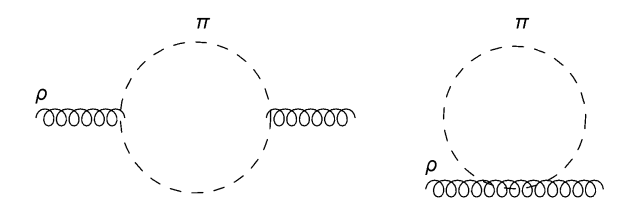


Fig. 1. Vacuum pion loops contributing to the  $\rho$  self-energy to leading order in the coupling constant (left panel:  $\pi\pi$ -loop, right panel: tadpole loop).

The task of computing the EM spectral function is thus converted into calculating the  $\rho$  spectral function which is given in terms of its self-energy,  $\Sigma_{\rho}^{\mu\nu}$ . In vacuum, the latter is generated by the  $\rho$ 's 2-pion cloud, including its 2-pion decay with a branching ratio of near 100%. At finite temperature, the pions are subject to rescattering off thermal-medium particles, which we will approximate by a pion gas. We will discuss those two cases in the following sections.

#### 2.2. Rho meson in vacuum

When gauging the free pion Lagrangian with a  $\rho$  meson using minimal substitution, and adding the  $\rho$ -meson mass and field-strength terms, one obtains the following effective Lagrangian for the  $\pi$ - $\rho$  system:

$$\mathcal{L}_{\pi} + \mathcal{L}_{\rho} = \frac{1}{2} \partial_{\mu} \vec{\phi} \cdot \partial^{\mu} \vec{\phi} - \frac{1}{2} m_{\pi}^{2} \vec{\phi} \cdot \vec{\phi} - \frac{1}{4} \rho_{\mu\nu} \rho^{\mu\nu} + \frac{1}{2} (m_{\rho}^{(0)})^{2} \rho_{\mu} \rho^{\mu}, \tag{5}$$

$$\mathcal{L}_{\pi\rho} = \frac{1}{2} i g_{\rho} \rho_{\mu} (T_3 \vec{\phi} \cdot \partial^{\mu} \vec{\phi} + \partial^{\mu} \vec{\phi} \cdot T_3 \vec{\phi}) - \frac{1}{2} g_{\rho}^2 \rho_{\mu} \rho^{\mu} T_3 \vec{\phi} \cdot T_3 \vec{\phi}. \tag{6}$$

Here,  $\rho_{\mu\nu}=\partial_{\mu}\rho_{\nu}-\partial_{\nu}\rho_{\mu}$ ,  $T_{3}=-i\epsilon_{3ab}$ , and  $m_{\pi}=140\,\mathrm{MeV}$  is the pion mass. To leading order in the gauge coupling constant,  $g_{\rho}$ , the vacuum  $\rho$  propagator, with a "bare mass  $m_{\rho}^{(0)}$ , receives two contributions, diagrammatically depicted in Fig. 1. The first one, the  $\pi\pi$ -loop, gives rise to the vacuum  $\rho\to\pi\pi$  decay, while the purely real "tadpole" diagram produces a constant shift in the  $\rho$  mass. However, the tadpole is essential to ensure a 4-dimensionally transverse  $\rho$  self-energy,  $q_{\mu}\Sigma_{\rho}^{\mu\nu}=0$  [29].

From the Lagrangian, the free pion propagator,  $D_{\pi}$ ,  $\rho\pi\pi$  vertex,  $\Gamma^{(3)}_{\mu(ab)}$ , and  $\rho\rho\pi\pi$  vertex,  $\Gamma^{(4)}_{\mu\nu(ab)}$ , follow as:

$$D_{\pi}(k) = \frac{1}{k^2 - m_{\pi}^2 + i\epsilon},\tag{7}$$

$$\Gamma_{\mu abc}^{(3)} = g_{\rho} \epsilon_{cab} (2k+q)_{\mu}, \tag{8}$$

$$\Gamma^{(4)}_{\mu\nu\,abcd} = ig_{\rho}^2 (2\delta_{ab}\delta_{cd} - \delta_{ac}\delta_{bd} - \delta_{ad}\delta_{bc})g_{\mu\nu} , \qquad (9)$$

where Greek (Roman) indices are used to denote Lorentz (isospin) space. Fig. 2 displays the propagators and vertices diagrammatically. The  $\rho$  self-energy energy diagrams can be evaluated as

$$\Sigma_{\rho}^{\mu\nu}(q) = \frac{-i}{2} \int \frac{d^4k}{(2\pi)^4} D_{\pi}(k) D_{\pi}(q+k) \Gamma_{\mu 3ab}^{(3)}(k,q) \Gamma_{\mu 3ba}^{(3)}(q+k,-q) - \frac{1}{2} \int \frac{d^4k}{(2\pi)^4} D_{\pi}(k) \Gamma_{\mu\nu aa33}^{(4)}(k,q) .$$
 (10)

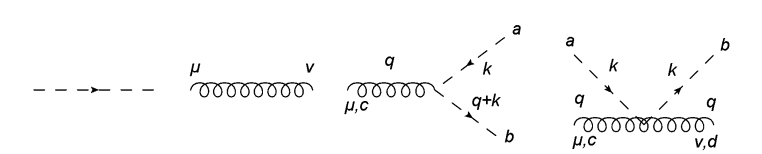


Fig. 2. From left to right:  $\pi$ -propagator,  $\rho$ -propagator,  $\rho\pi\pi$  vertex, and  $\pi\pi\rho\rho$  vertex.

A symmetry factor of  $\frac{1}{2}$  has been added to both terms to remove double counting of pion states, since the different pions are distinguishable in particle space (different charge states), but not in isospin space.

To regularize the loop integrals for  $\Sigma_{\rho}^{\mu\nu}$  we employ the Pauli-Villars scheme as a means to maintain gauge invariance [29,32]. In this scheme,  $\rho$  self-energies are calculated by subtracting "heavy-pion" propagators from the physical ones in the unregularized self-energy, yielding

$$\Sigma_{\rho}^{\prime\mu\nu}(q) = \Sigma_{\rho}^{\mu\nu}(q, m_{\pi}) - 2\Sigma_{\rho}^{\mu\nu}(q, \sqrt{m_{\pi}^2 + \Lambda_0^2}) + \Sigma_{\rho}^{\mu\nu}(q, \sqrt{m_{\pi}^2 + 2\Lambda_0^2}). \tag{11}$$

We adopt the values of  $g_{\rho} = 5.9$ ,  $m_{\rho}^{(0)} = 853$  MeV, and  $\Lambda_0 = 1$  GeV, which have been previously fitted to the *P*-wave  $\pi\pi$  phase shifts and pion electromagnetic form factor [26].

Finally,  $\Sigma_{\rho}^{\prime\mu\nu}$  can be resummed into the vacuum  $\rho$  propagator yielding [29]:

$$D_{\rho}^{\mu\nu}(k) = D_{\rho}(k)(-g^{\mu\nu} + \frac{k^{\mu}k^{\nu}}{k^2}) + \frac{k^{\mu}k^{\nu}}{(m_{\rho}^{(0)})^2k^2},\tag{12}$$

$$D_{\rho}(k) = \frac{1}{k^2 - (m_{\rho}^0)^2 - \Sigma_{\rho}'(k)},\tag{13}$$

$$\Sigma_{\rho}^{\prime\mu\nu}(k) = (-g^{\mu\nu} + \frac{k^{\mu}k^{\nu}}{k^2})\Sigma_{\rho}^{\prime}(k) . \tag{14}$$

In the following, we drop the prime notation from the regularized  $\rho$  self-energy.

# 2.3. General form of $\rho$ self-energy at finite temperature

We calculate  $\Sigma_{\rho}^{\mu\nu}$  at finite temperature within the imaginary-time formalism, using the methods outlined in Refs. [33,34]; one obtains

$$\Sigma_{\rho}^{\mu\nu}(q) = g_{\rho}^{2} \int \frac{d^{3}k}{(2\pi)^{3}} \int_{-\infty}^{\infty} \frac{dv dv'}{\pi^{2}} \frac{(2k+q)^{\mu}(2k+q)^{\nu}}{q_{0}+v-v'+i\epsilon} \text{Im}[D_{\pi}(v,\vec{k})]$$

$$\times \text{Im}[D_{\pi}(v',\vec{k}+\vec{q})](f(v)-f(v')) + I_{\text{Tad}}, \qquad (15)$$

where

$$I_{\text{Tad}} = \frac{g_{\rho}^2 g^{\mu \nu}}{4\pi^4} \int d^3 k \int_{-\infty}^{\infty} dv \text{Im}[D_{\pi}(v, \vec{k})] f(v) . \tag{16}$$

The first term is complex, while the second is purely real. The imaginary part of  $\Sigma_{\rho}^{\mu\nu}$  can be slightly simplified as

$$\operatorname{Im}\Sigma_{\rho}^{\mu\nu}(q) = g_{\rho}^{2} \int \frac{d^{3}k}{(2\pi)^{3}} \int_{0}^{q_{0}} \frac{dv}{-\pi} \operatorname{Im}[D_{\pi}(v,\vec{k})] \operatorname{Im}[D_{\pi}(q_{0}-v,\vec{q}+\vec{k})]$$

$$\times (2k+q)^{\mu} (2k+q)^{\nu} (1+f(v)+f(q_{0}-v))$$

$$+2g_{\rho}^{2} \int \frac{d^{3}k}{(2\pi)^{3}} \int_{0}^{\infty} \frac{dv}{-\pi} \operatorname{Im}[D_{\pi}(v,\vec{k})] \operatorname{Im}[D_{\pi}(q_{0}+v,\vec{q}+\vec{k})]$$

$$\times (2k+q)^{\mu} (2k+q)^{\nu} (f(v)-f(q_{0}+v)), \qquad (17)$$

where we have separated the self-energy into two "cuts". The first integral corresponds to the unitarity cut, which represents the vacuum  $\rho \to \pi\pi$  decay and its Bose enhancement, while the second integral is referred to as Landau cut which represents  $\rho\pi$  scattering through an intermediate pion state. The energy dependent part of the real part of  $\Sigma_{\rho}^{\mu\nu}$  can be calculated from a dispersion relation, while the constant shift from the tadpole diagram can be calculated directly as

$$\operatorname{Re}\Sigma_{\rho}^{\mu\nu}(q) = \frac{-1}{\pi} \text{p.v.} \int_{0}^{\infty} dv^{2} \frac{1}{q_{0}^{2} - v^{2}} \operatorname{Im}\Sigma_{\rho}^{\mu\nu}(v, \vec{q}) + I_{\text{Tad}},$$
 (18)

where p.v. indicates the principal value of the integral.

At finite temperature the breaking of Lorentz invariance splits the  $\rho$  propagator at finite 3-momentum into transverse and longitudinal modes that can be expressed in terms of projection operators  $P_T^{\mu\nu}$  and  $P_L^{\mu\nu}$  as [35]

$$D_{\rho}^{\mu\nu}(q,T) = \frac{P_{T}^{\mu\nu}}{M^{2} - (m_{\rho}^{0})^{2} - \Sigma_{\rho}^{T}(q,T)} + \frac{P_{L}^{\mu\nu}}{M^{2} - (m_{\rho}^{0})^{2} - \Sigma_{\rho}^{L}(q,T)} + \frac{q^{\mu}q^{\nu}}{(m_{\rho}^{0})^{2}M^{2}}, \quad (19)$$

where  $M^2 = q_0^2 - \vec{q}^2$  is the  $\rho$  meson's invariant mass. The projection operators are defined by

$$P_T^{\mu\nu} = 0$$
, for  $\mu = 0$  or  $\nu = 0$ ,

$$P_T^{\mu\nu} = \delta^{\mu\nu} - \frac{q^{\mu}q^{\nu}}{\vec{q}^2}, \text{ for } \mu, \nu \in \{1, 2, 3\},$$
 (20)

$$P_L^{\mu\nu} = \frac{q^{\mu}q^{\nu}}{M^2} - g^{\mu\nu} - P_T^{\mu\nu} \,. \tag{21}$$

The transverse and longitudinal components of the rho self-energy,  $\Sigma_{\rho}^{T}$  and  $\Sigma_{\rho}^{L}$ , follow as

$$\Sigma_{\rho}^{\mu\nu}(q,T) = P_{T}^{\mu\nu} \Sigma_{\rho}^{T}(q,T) + P_{L}^{\mu\nu} \Sigma_{\rho}^{L}(q,T). \tag{22}$$

For  $\vec{q} = 0$ ,  $\Sigma_T(q_0, T) = \Sigma_L(q_0, T)$ , allowing one to write the conductivity in terms of only the transverse projection of the rho self-energy:

$$\sigma_{\rm el} = \frac{e^2}{g_{\rho}^2} \lim_{q_0 \to 0} \operatorname{Im} \left[ \frac{-(m_{\rho}^0)^4}{q_0^2 - (m_{\rho}^0)^2 - \sum_{\rho}^T (q_0, \vec{q} = 0)} \right]. \tag{23}$$

### 2.4. On-shell pion approximation

For very small energies  ${\rm Im}D_{\rho}$  is approximately proportional to  ${\rm Im}\Sigma_{\rho}^T$ , which is dominated by the Landau cut below  $q_0\approx 2m_\pi$ . Therefore the conductivity can be approximated as

$$\sigma_{\rm el} \approx \frac{-2e^2}{3} \int \frac{d^3k}{(2\pi)^3} \int_0^\infty \frac{dv}{-\pi} [\text{Im} D_\pi(v, \vec{k})]^2 \times \frac{4|\vec{k}|^2 e^{\frac{v}{T}}}{T(-1 + e^{\frac{v}{T}})^2} , \qquad (24)$$

where we have taken the limit  $q_0 \to 0$  analytically. We see that one must introduce a finite pion width into  $D_\pi$  in order to obtain a finite conductivity. This implies that we have to include at least two thermal-pion insertions in order to obtain a result beyond the ideal-gas limit. One can approximate the conductivity using a small, but finite, pion width,  $\Gamma_\pi$ . In this approximation the pion propagator becomes

$$D_{\pi}(k) = \frac{1}{2\omega_k} \sum_{+} \frac{\pm 1}{k_0 \mp \omega_k + i\frac{\Gamma_{\pi}}{2}},$$
 (25)

with  $\omega_k = \sqrt{k^2 + m_\pi^2}$ . In the small-width limit  $[\text{Im}D(k)]^2$  is approximately

$$[\operatorname{Im}D(k)]^{2} \approx \frac{\pi}{4\omega_{k}^{2}} \frac{1}{\Gamma_{\pi}} \delta(k_{0} - \omega_{k}) . \tag{26}$$

One can use Eqs. (24) and (26) to show that

$$\sigma_{\rm el} = \frac{2e^2}{3T} \int \frac{d^3\vec{k}}{(2\pi)^3} \frac{v_k^2}{\Gamma_{\pi}} f(\omega_k) (1 + f(\omega_k)) , \qquad (27)$$

where  $v_k = |\vec{k}|/\omega_k$  is the pion's velocity. This result agrees with similar calculations where the conductivity is expressed in terms of the pion width [10,17,36].

#### 3. Thermal $\pi\pi$ scattering

In this section we calculate the pion self-energy due to thermal S- and P-wave  $\pi\pi$  scattering. The self-energy can be resummed into a thermal pion propagator yielding

$$D_{\pi}(k_0, \vec{k}) = \frac{1}{k^2 - m_{\pi}^2 + \Sigma_{\pi}(k, T)} \ . \tag{28}$$

We first obtain the self-energy expression from the Matsubara formalism in terms of the  $\pi\pi$  scattering amplitude (Sec. 3.1), discuss the implementation of phenomenological vertex form factors (Sec. 3.2) and constraints from vacuum  $\pi\pi$  phase shifts and cross sections (Sec. 3.3), and finally present our numerical results for the pion optical potentials in a hot pion gas (Sec. 3.4).

### 3.1. Pion self-energy

Assuming the dominance of s-channel resonances we are able to describe S- and P-wave  $\pi\pi$  interactions up to center-of-mass (CM) energies of about 1 GeV [37], which is sufficient for the typical temperatures under consideration. Such scatterings can be fairly well approximated through  $\sigma(500)$  and  $\rho(770)$  resonances, whose pertinent diagrams are illustrated in Fig. 3. We use the vertices and propagators established in Sec. 2.2 to construct the pion self-energy for  $\pi\pi$  scattering through a  $\rho$  resonance, while we follow the approach outlined in Refs. [34,37] to calculate scattering through an effective  $\sigma(500)$  resonance. The in-medium pion self-energies  $(R = \sigma, \rho)$  are then obtained as

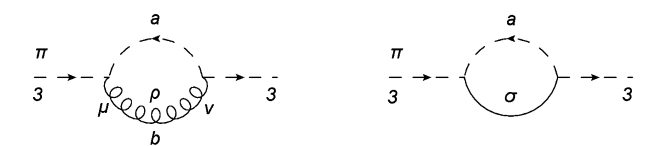


Fig. 3. The pion self-energy resulting from resonant scattering of a pion with a thermal pion through intermediate  $\rho$  (left) and  $\sigma$  (right) mesons.

$$\Sigma_{\pi}^{R}(k) = g_{R}^{2} \int \frac{d^{3}p}{(2\pi)^{3}} \int_{-\infty}^{\infty} \frac{dwdw'}{\pi^{2}} \left[ \text{Im}[D_{\pi}(w, \vec{p})] \text{Im}[D_{R}(w', \vec{k} + \vec{p})] \right] \times \frac{N_{R\pi\pi}[p, k, w'] \text{FF}_{R}(q_{\text{CM}}^{2})(f(w) - f(w'))}{k_{0} + w - w' + i\epsilon} \Big]_{p_{0} = w}$$
(29)

with the vertex functions

$$N_{\rho\pi\pi}[p,k,w'] = -(k-p)^2 + \frac{(k^2 - p^2)^2}{w'^2 - (\vec{p} + \vec{k})^2}$$
(30)

and

$$N_{\sigma\pi\pi}[p,k,w'] = \frac{w'^2 - (\vec{k}+\vec{p})^2 - m_{\pi}^2}{2} \,. \tag{31}$$

The vacuum  $\rho$  propagator,  $D_{\rho}^{\mu\nu}$ , is taken from Eq. (12) and  $D_{\sigma}$  is the vacuum  $\sigma$  (500) propagator,

$$D_{\sigma}(E) = \frac{1}{E^2 - m_{\sigma}^2 - \Sigma_{\sigma}(E)},$$
(32)

where  $m_{\sigma}$  is the bare sigma mass and  $\Sigma_{\sigma}$  its vacuum self-energy,

$$\Sigma_{\sigma}(E) = 3g_{\sigma}^{2} \int \frac{d|\vec{k}|\vec{k}^{2}}{(2\pi)^{2}} \frac{(E^{2} - m_{\pi}^{2})FF_{\sigma}(k)^{2}}{\omega_{k}(E^{2} - 4\omega_{k}^{2} + i\epsilon)}.$$
(33)

Although we dress the intermediate  $\rho(770)$  and  $\sigma(500)$  propagators in  $\Sigma_{\pi}$  with their vacuum self-energies, the pion propagators within  $\Sigma_{\pi}$  are not dressed. These propagators will not induce an infinite conductivity, because they correspond to thermal pions, while only intermediate particle states transmit charge through the medium.

#### 3.2. Form factor

Phenomenological form factors  $FF_R$  at each vertex are a standard tool to simulate the finitesize effects of hadrons while also regularizing vacuum loop integrals. For the purpose of the  $\pi\pi$ scattering amplitude we do not employ the Pauli-Villars scheme (which is not necessary) but resort to a simpler form given by

$$FF_{\rho}(q_{\text{CM}}) = \frac{\Lambda_{\rho}^2 + m_{\rho}^2}{\Lambda_{\rho}^2 + 4(m_{\pi}^2 + q_{\text{CM}}^2(p, k))}$$
(34)

$$FF_{\sigma}(q_{CM}) = \frac{\Lambda_{\sigma}^{2}}{\Lambda_{\sigma}^{2} + 4(m_{\pi}^{2} + q_{CM}^{2}(p, k))}$$
(35)

$$q_{\text{CM}}^2(p,k) = \frac{((p+k)^2 - k^2 - p^2)^2 - 4k^2p^2}{4(p+k)^2} , \tag{36}$$

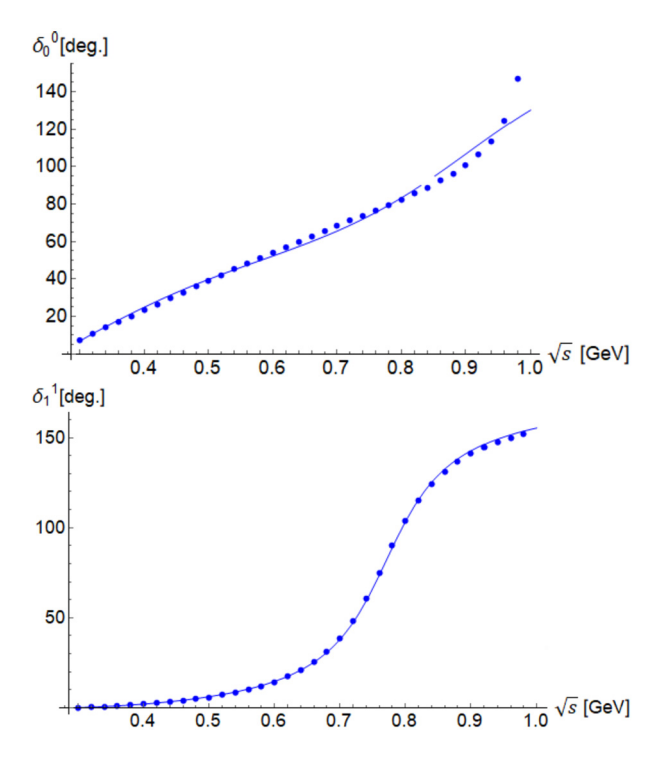


Fig. 4. Fits to the isoscalar S- (upper panel) and isovector P-wave (lower panel)  $\pi\pi$  scattering phase shift via  $\sigma$  and  $\rho$  resonance scattering, respectively, compared to experimental data [38].

where  $q_{\rm CM}$  is pion momentum in the CM system of the collision. In the following section we constrain the parameters of the  $\pi\pi$  amplitudes through vacuum scattering data.

### 3.3. Comparisons to vacuum data

For comparisons to vacuum scattering data the pion energies,  $k_0$  and  $p_0$ , are taken to be onshell, while the CM energy,  $E_{\rm CM}=\sqrt{s}$ , is taken as an external variable. The CM momentum is then given by

$$q_{\rm CM}(s) = \sqrt{\frac{s}{4} - m_{\pi}^2} \ . \tag{37}$$

From the vacuum resonance self-energies, the  $\pi\pi$  scattering phase shift in the pertinent resonance channel  $(R = \rho, \sigma)$  can be obtained as

$$\tan \delta_R(E_{\rm CM}) = -\frac{{\rm Im}\Sigma_R(E_{\rm CM})}{{\rm Re}\Sigma_R(E_{\rm CM})} \,. \tag{38}$$

We utilize these data to fit our parameters resulting to describe the S- and P-wave  $\pi\pi$  scattering phase shifts [38]. The fits are shown in Fig. 4 based on the values:  $g_{\sigma}=8.86$ ,  $m_{\sigma}=0.934\,\mathrm{GeV}$ ,  $\Lambda_{\rho}=1.85\,\mathrm{GeV}$ , and  $\Lambda_{\sigma}=0.745\,\mathrm{GeV}$ . The fit quality is rather good up to CM energies of 1 GeV which is sufficient for our application to a thermal pion gas for temperatures of up to 180 MeV. Finally, we calculate the resulting elastic  $\pi\pi$  cross section by utilizing the optical theorem to express it through the imaginary part of the forward scattering amplitude  $M_{\pi\pi}$ ,

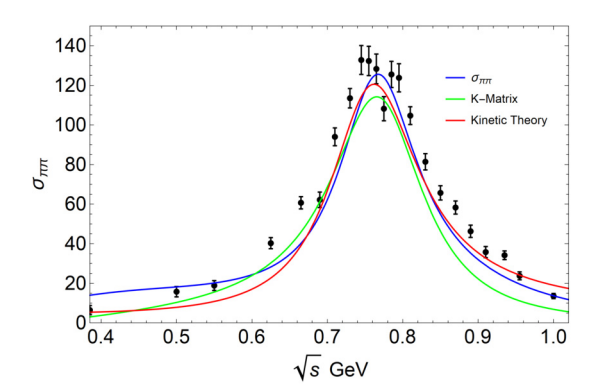


Fig. 5. Comparison of our  $\pi\pi$  cross section (blue) to experimental data (black dots) [39] and two previous works with applications to the electric conductivity: Breit-Wigner ansatz for the  $\rho$ -resonance cross section (red) [8], K-matrix formalism (green) [16]. (For interpretation of the colors in the figure(s), the reader is referred to the web version of this article.)

$$\sigma_{\pi\pi}(s) = -\frac{(1)}{\sqrt{s(s - 4m_{\pi}^2)}} \text{Im}[M_{\pi\pi}(s)], \qquad (39)$$

where the amplitude for a given spin-isospin channel can be related to the resonance propagator as

$$M_{\pi\pi}^{00}(s) = \frac{g_{\sigma}^2}{2}(s - m_{\pi}^2)D_{\sigma}(s)FF_{\sigma}(q_{\text{CM}}^2)$$
(40)

$$M_{\pi\pi}^{11}(s) = g_{\rho}^{2}(s - 4m_{\pi}^{2})D_{\rho}(s)FF_{\rho}(q_{CM}^{2}). \tag{41}$$

In Fig. 5 we compare our cross section to experimental data [39], and to several other works where it was also used as an input to calculating the electric conductivity [8,16]. The  $\rho$  resonance peak in our cross section turns out to be somewhat narrower than experimental data, a feature that is apparently shared by other calculations and possibly related to the absence of non-resonant "background" terms.

### 3.4. Optical potentials

To obtain the in-medium pion self energy we first compute the imaginary part directly from Eq. (29) and subsequently the real part from a subtracted dispersion relation,

$$\operatorname{Re}\Sigma_{\pi}(k) = \int_{-\infty}^{\infty} \frac{dw}{-\pi} \left( \frac{\operatorname{Im}\Sigma_{\pi}(w,\vec{k})}{k_0 - w} - \frac{\operatorname{Im}\Sigma_{\pi}(w,\vec{k})}{-w} \right). \tag{42}$$

The subtraction ensures that  $\text{Re}\Sigma_{\pi}$  is zero for zero energy. This is motivated by the pion being a Goldstone boson, to approximately implement chiral constraints on the low-energy behavior of the amplitudes [27,37]. A convenient and more intuitive way to represent the pion self-energy, whose dimension is quadratic in energy, is to define corresponding "optical potentials", which formally can be thought of as resulting from the leading-order corrections to the pion's dispersion relation. Their on-shell values take the form

$$U_{\pi}(\vec{k}) = \Sigma_{\pi}(\omega_k, \vec{k})/2\omega_k , \qquad (43)$$

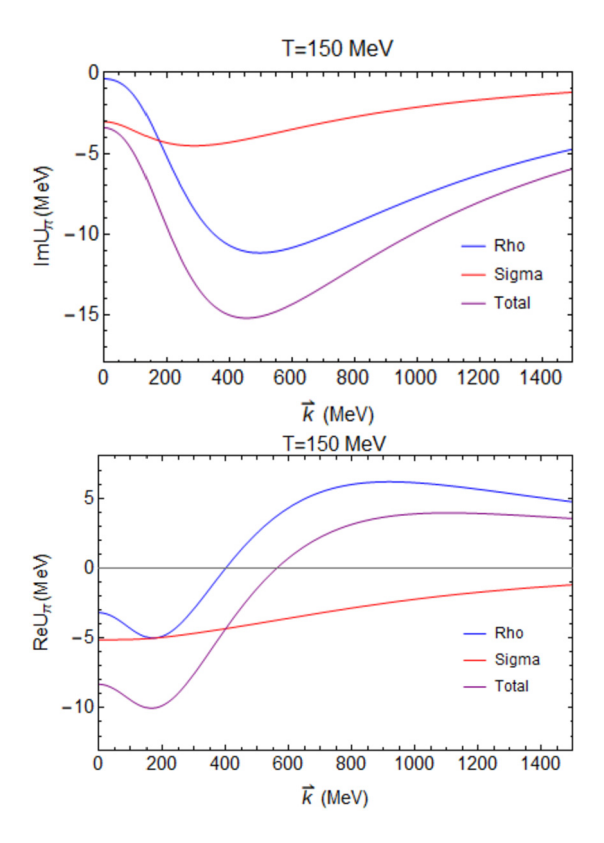


Fig. 6. Imaginary (upper panel) and real part (lower panel) of the on-shell pion optical potential in hot pion matter, plotted as a function of 3-momentum for  $T=150\,\mathrm{MeV}$ . Contributions from the rho (blue) and sigma (red) resonances are shown in addition to the total (purple).

representing the real and imaginary parts of the in-medium contributions to the on-shell pion self-energy (also note that  $-2 \text{Im} U_{\pi}$  amounts to the Breit-Wigner width,  $\Gamma_{\pi}$  (or full-width-half-maximum), around the on-shell pole in the spectral function) We graph the real and imaginary parts of the optical potential in Fig. 6; they generate a pion mass shifts of up to  $\pm 10$  MeV, and pion widths of up to 30 MeV. This is in rather good agreement with the results of Refs. [27,40] for the  $\sigma$  and  $\rho$  channels. However, for momenta of up to  $\sim 1$  GeV the imaginary part of our total pion self-energy is a few MeV smaller than that obtained in the previous work, because the latter also contains non-resonant S-wave and D-wave contributions. As these contributions lead to additional complications with preserving gauge invariance, while their quantitative impact is only at the 10% level, we neglect them for now.

### 4. Gauge invariance in medium

In this section we scrutinize the issue of gauge invariance, that is violated when introducing in-medium pion self-energies and therefore needs to be restored by accounting for pertinent vertex corrections. Toward this end, we first introduce in Sec. 4.1 the Ward identities between 2-, 3- and 4-point functions in our model that provide a sufficient criterion for a gauge invariant set of diagrams. In Sec. 4.2 we lay out the general strategy of how the pertinent vertex functions can

be constructed. In Sec. 4.3 we address the complications associated with having to dress intermediate propagators inside the vertex corrections which is dictated by rendering the conductivity finite, while in Sec. 4.4 we elaborate on how to approximately maintain gauge invariance in the presence of form factors that figure in the vertex corrections. Finally, in Sec. 4.5 we summarize our expression for the transverse  $\rho$  self-energy in compact form at vanishing 3-momentum that will be used for the calculation of the conductivity.

### 4.1. Ward identities

In the VDM the  $\rho$  meson couples to a conserved current, and thus must be four-dimensionally transverse,  $q_{\mu} \Sigma_{\rho}^{\mu\nu} = 0$ . Transversality is ensured if the  $\rho\pi\pi$  and  $\rho\rho\pi\pi$  vertices satisfy the Ward-Takahashi identities between the 2-point and 3-point functions, as well as the 3-point and 4-point functions in the model, *i.e.*,

$$q^{\mu}\Gamma^{(3)}_{\mu ab3} = g_{\rho}\epsilon_{3ab}(D_{\pi}^{-1}(k+q) - D_{\pi}^{-1}(k)), \qquad (44)$$

$$q^{\mu}\Gamma_{\mu\nu\,ab33}^{(4)} = ig_{\rho}(\epsilon_{3ca}\Gamma_{\nu\,bc3}^{(3)}(k, -q) - \epsilon_{3bc}\Gamma_{\nu\,ca3}^{(3)}(k + q, -q)). \tag{45}$$

The Ward-Takahashi identities are straightforwardly satisfied in vacuum, but are upset by the introduction of a thermal pion self-energy in  $D_{\pi}$ . This can be remedied by considering thermal corrections to the  $\rho\pi\pi$  and  $\rho\rho\pi\pi$  vertices [28,32]. Following these references, the in-medium vertices can be written as

$$\Gamma^{(3)}_{\mu ab3} = g_{\rho} \epsilon_{3ab} (2k+q)_{\mu} + \Gamma^{\prime (3)}_{\mu ab3} , \qquad (46)$$

$$\Gamma^{(4)}_{\mu\nu ab33} = 2ig_{\rho}^{2}(\delta_{ab} - \delta_{3a}\delta_{3b})g_{\mu\nu} + \Gamma^{(4)}_{\mu\nu ab33}, \qquad (47)$$

where  $\Gamma_{\mu\,ab3}^{\prime\,(3)}$  and  $\Gamma_{\mu\nu\,ab3}^{\prime\,(4)}$  are vertex corrections to the  $\rho\pi\pi$  and  $\rho\rho\pi\pi$  vertices. The Ward identities will hold if the vertex corrections satisfy

$$q^{\mu}\Gamma_{\mu ab3}^{\prime(3)} = g_{\rho}\epsilon_{3ab}(\Sigma_{\pi}(k) - \Sigma_{\pi}(k+q)), \tag{48}$$

$$q^{\mu}\Gamma_{\mu\nu ab33}^{\prime(4)} = ig_{\rho}(\epsilon_{3ca}\Gamma_{\nu bc3}^{\prime(3)}(k, -q) - \epsilon_{3bc}\Gamma_{\nu ca3}^{\prime(3)}(k + q, -q)), \tag{49}$$

In the following, we will use these as our guiding principle.

#### 4.2. Vertex corrections

The corrections to the  $\rho\pi\pi$  vertex sufficient to satisfy the Ward identities can be generated by coupling a  $\rho$  meson (or photon) to all possible charged-particle lines in  $\Sigma_{\pi}$ . Similarly, one can couple two  $\rho$  mesons to  $\Sigma_{\pi}$  in all possible configurations to obtain corrections to the  $\rho\rho\pi\pi$  vertex [32]. We then analytically determine which vertex corrections are necessary to maintain the Ward identities when  $D_{\pi}$  is dressed with only thermal  $\pi\pi$  scattering. Figs. 7 through 9 show the vertex corrections resulting from dressing  $D_{\pi}$  with  $\Sigma_{\pi}^{(\rho)}$  and  $\Sigma_{\pi}^{(\sigma)}$ . We show only the minimum diagrams necessary to maintain gauge invariance. Consequently, there are fewer corrections for the  $\sigma$  resonance interactions, because the  $\sigma$  meson is neutral and the  $\sigma\pi\pi$  vertex is a Lorentz scalar. Furthermore, the vertex corrections require the  $\rho\rho\rho$ ,  $\rho\rho\rho\rho$ , and  $\sigma\pi\pi$  vertices. Terms including the  $\rho\rho\rho$  or  $\rho\rho\rho\rho$  vertex contain multiple  $\rho$  propagators, and are therefore suppressed by  $1/m_{\rho}^2$ . Thus we drop all corrections containing these vertices and do not write them here.

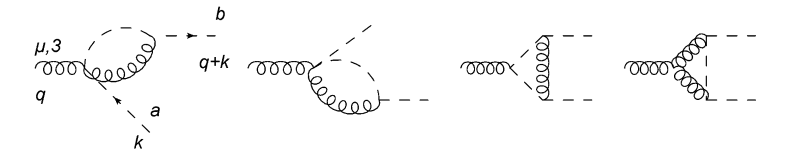


Fig. 7. Corrections to the  $\rho\pi\pi$  vertex due to  $\Sigma_{\pi}^{(\rho)}$ .

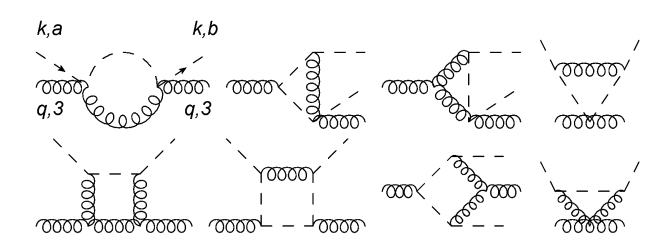


Fig. 8. Corrections to the  $\rho\rho\pi\pi$  vertex due to  $\Sigma_{\pi}^{(\rho)}$ .

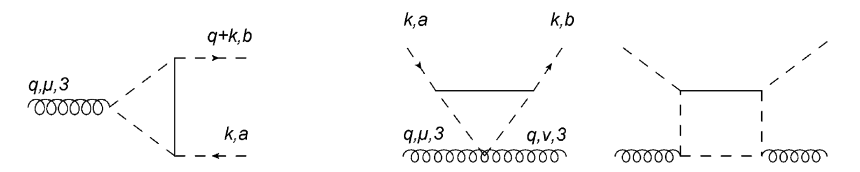


Fig. 9. Left panel: Correction to the  $\rho\pi\pi$  vertex due to  $\Sigma_{\pi}^{(\sigma)}$ . Right panels: Corrections to the  $\rho\rho\pi\pi$  vertex due to  $\Sigma_{\pi}^{(\sigma)}$ .

In order to calculate vertex corrections involving a  $\sigma$  meson we introduce an effective  $\sigma\pi\pi$  vertex that corresponds to our calculation of the vacuum self-energy of the  $\sigma$  meson through  $\pi\pi$  loops in Sec. 3.1,

$$\Gamma_{\sigma ab}^{(3)} = i\delta_{ab}g_{\sigma}\sqrt{s - m_{\pi}^2} , \qquad (50)$$

which reproduces our results for  $\Sigma_{\sigma}$  and  $\Sigma_{\pi}^{(\sigma)}$ . The expression for  $\Gamma_{\sigma ab}^{(3)}$  can then be used to calculate vertex corrections involving the  $\sigma\pi\pi$  vertex. We calculate all diagrams resulting from replacing a vacuum vertex with a corresponding vertex correction. For the four-point vertex corrections, we also include diagrams resulting from interchanging  $\rho$ -meson or pion propagators when they produce unique vertex corrections.

### 4.3. Dressing intermediate particles

The vertex corrections contain intermediate  $\rho$ ,  $\sigma$ , and pion propagators. As we have seen for the Landau cut of  $\Sigma_{\rho}^{\mu\nu}$ , if these propagators are not dressed, the conductivity will diverge. Therefore, we dress the  $\rho$  and  $\sigma$  propagators with their vacuum self-energies and treat the intermediate-pion propagators self-consistently, *i.e.*,

$$D_{\pi}(k) = \frac{1}{k^2 - m_{\pi}^2 - \Sigma_{\pi}(k)} \ . \tag{51}$$

However, thermal pions within vertex corrections and the pion self-energy are not dressed. The widths in the pion and  $\rho$  propagators cause another layer of violation of gauge invariance. However, the violation due to dressing  $D_{\rho}$  only occurs in vertex corrections containing multiple  $\rho$  propagators, which are suppressed by powers of  $1/m_{\rho}$ . The violation due to dressing intermediate-pion propagators within vertex corrections can be corrected by dressing the  $\rho\pi\pi$ vertices that couple to an external  $\rho$  with three point-vertex corrections and dressing thermalpion propagators, creating a self-consistency equation. These effects are expected to be small, due to the small pion width, thus we will not calculate these corrections in this work.

### 4.4. Vertex correction form factors

In Ref. [32] the in-medium dressing of the pions with nucleons and  $\Delta(1232)$ 's was implemented in a non-relativistic approximation, so that the corresponding form factors depended only on the pion's three-momentum (the lab frame momentum). The form factors were generated by attaching heavy pions to the external pions in  $\Sigma_{\pi}$  and the vertex corrections. These form factors violated the Ward identities, however, this violation was corrected by including further vertex corrections, derived by coupling  $\rho$  mesons directly to heavy-pion propagators [32]. The additional vertex corrections could be expressed in terms of the pion self-energy and the original corrections to the  $\rho\pi\pi$  vertex. Two complications arise when applying the regularization procedure from Ref. [32] with the form factors introduced in Sec. 3.2. First, different form factors were introduced for the S- and P-wave contributions to the self-energy, and second, the CM momentum was used to as the variable.

In order to extend the approach of Ref. [32] to multiple form factors we note that  $\Sigma_{\pi}^{(\rho)}$  and its vertex corrections,  $\Gamma^{\prime\,(3)\rho}_{\mu\,ab3}$  and  $\Gamma^{\prime\,(4)\rho}_{\mu\nu\,ab33}$ , independently satisfy Eqs. (48) and (49), such that

$$q^{\mu}\Gamma^{\prime(3)\rho}_{\mu ab3} = g_{\rho}\epsilon_{3ab}(\Sigma^{(\rho)}_{\pi}(k) - \Sigma^{(\rho)}_{\pi}(k+q))$$
(52)

$$q^{\mu}\Gamma_{\mu ab3}^{\prime(3)\rho} = g_{\rho}\epsilon_{3ab}(\Sigma_{\pi}^{(\rho)}(k) - \Sigma_{\pi}^{(\rho)}(k+q))$$

$$q^{\mu}\Gamma_{\mu\nu ab33}^{\prime(4)\rho} = ig_{\rho}(\epsilon_{3ca}\Gamma_{\nu bc3}^{\prime(3)\rho}(k,-q) - \epsilon_{3bc}\Gamma_{\nu ca3}^{\prime(3)\rho}(k+q,-q)) .$$
(52)

Similarly,  $\Sigma_{\pi}^{(\sigma)}$  and its vertex corrections,  $\Gamma_{\mu \, ab3}^{\prime \, (3)\sigma}$  and  $\Gamma_{\mu \, \nu \, ab33}^{\prime \, (4)\sigma}$ , satisfy

$$q^{\mu}\Gamma_{\mu ab3}^{\prime(3)\sigma} = g_{\rho}\epsilon_{3ab}(\Sigma_{\pi}^{(\sigma)}(k) - \Sigma_{\pi}^{(\sigma)}(k+q))$$

$$\tag{54}$$

$$q^{\mu}\Gamma_{\mu ab3}^{\prime(3)\sigma} = g_{\rho}\epsilon_{3ab}(\Sigma_{\pi}^{(\sigma)}(k) - \Sigma_{\pi}^{(\sigma)}(k+q))$$

$$q^{\mu}\Gamma_{\mu\nu ab33}^{\prime(4)\sigma} = ig_{\rho}(\epsilon_{3ca}\Gamma_{\nu bc3}^{\prime(3)\sigma}(k,-q) - \epsilon_{3bc}\Gamma_{\nu ca3}^{\prime(3)\sigma}(k+q,-q)) .$$
(54)

One realizes that the  $\sigma$  and  $\rho$  resonances form subgroups that independently satisfy the Ward identities. Thus, the regularization procedure from Ref. [32] can be applied separately to S- and P-wave scattering. The total regularized vertex corrections are then given by the sum of the corrections for each resonance.

Next we address the use of the CM momentum in the form factor. For  $\pi\pi$  scattering we cannot apply the non-relativistic approximations which mandated to employ a form factor depending on the CM momentum,  $q_{\rm CM}$ . Furthermore, the dependence on  $q_{\rm CM}$ , rather than  $\vec{k}$ , prevents the introduction of spurious total-momentum dependencies. While the use of  $q_{\rm CM}$  renders the pion self-energy more robust, it is not clear how to satisfy the Ward identities in this framework. However, the violation of the Ward identities is proportional to the difference in the  $q_{\rm CM}^2$  of the two pions in the  $\rho$  self-energy  $\pi\pi$  loop over  $\Lambda_R^2$ . Since we are chiefly interested in  $\sigma_{\rm el}$ , which involves the zero-momentum low-energy limit of the EM spectral function, the violation is parametrically suppressed, because  $\Lambda_R^2$  is on the order of several hundred MeV, while  $q_{\rm CM}$  is on the order of a few tens of MeV. This low energy suppression is expected because the form factors are constructed to suppress high-momentum behavior, while minimally affecting the low-momentum regime. Furthermore, to leading order the violation is proportional to  $q_0^2$  (where  $q_0$  is the  $\rho$ -meson's energy), while  $\Lambda_{\rho}$  is on the order of 1 GeV for the  $\rho$  resonance. Thus, the violation due to the form factors in  $\Sigma_{\pi(\rho)}$  should still be appreciably suppressed around the rho mass. Although  $\Lambda_{\sigma}=0.745$  GeV) is of the same order as  $m_{\rho}$ , the effects of  $\pi\pi$ -resonant scattering through a  $\sigma$  resonance on the EM spectral function are suppressed for large  $q_0$ . Therefore, the violation of gauge invariance due to using  $q_{\rm CM}$  in the form factor is expected to be small even for  $q_0$  around the rho mass.

Additionally, in order to further analyze the effect of the violation on our results, and provide an approximate correction for the violation, we follow the approach of Ref. [32] and generate additional vertex corrections involving heavy-pion propagators. However, at the vertices where a heavy-pion propagator couples to a thermal loop we replace the lab frame momentum,  $\vec{k}$ , with the center of mass momentum,  $q_{\text{CM}}$ . In Sec. 5 we will assess the effect of the additional vertex corrections on the EM spectral function, in order to quantify the effect this violation of gauge invariance has on our results.

The total vertex corrections to the  $\rho\pi\pi$  vertex, including terms where the  $\rho$  meson couples to a heavy-pion propagator, can then be written in terms of the original vertex corrections plus terms involving the pion self-energy. Similarly, the total corrections to the  $\rho\rho\pi\pi$  vertex can be written in terms of the original corrections plus terms involving the pion self-energy or the original vertex corrections to the  $\rho\pi\pi$  vertex. The regularized corrections to the  $\rho\pi\pi$  and  $\rho\rho\pi\pi$  vertices are written out in Appendix A.

## 4.5. $\rho$ self-energy at finite temperature

Here we write the transverse projection of  $\Sigma_{\rho}^{\mu\nu}$  for arbitrary  $\rho\pi\pi$  and  $\rho\rho\pi\pi$  vertices,  $\Gamma_{\mu\,ab3}^{(3)}(k,q)$  and  $\Gamma_{\mu\nu\,ab33}^{(4)}(k,q)$ , at  $\vec{q}=0$ :

$$\Sigma_{\rho}^{T}(q) = \frac{4\pi T}{3} \sum_{n(even)} \int \frac{d|\vec{k}|\vec{k}^{2}}{(2\pi)^{3}} D_{\pi}(k) \Big[ D_{\pi}(q+k) \Big( g_{\rho} \epsilon_{3ab}(2|\vec{k}|) + \Gamma_{3ab3}^{\prime(3)}(k,q) \Big) \\ \times \Big( g_{\rho} \epsilon_{3ba}(2|\vec{k}|) + \Gamma_{3ba3}^{\prime(3)}(k+q,-q) \Big) - \Big( \frac{3g_{\rho}^{2}}{\pi} + i \Gamma_{ii\,aa33}^{\prime(4)}(k,q) \Big) \Big]_{k_{0}=i\omega_{n}},$$
 (56)

where we have performed the angular integrations analytically, and  $\omega_n$  are discrete Matsubara frequencies. The vertex corrections are complex and introduce nontrivial energy dependence into the vertices, and thus must be written with a spectral representation, before Matsubara sums are performed. In appendix B we establish the relevant spectral representations and carry out the summations in eq. (56).

### 5. Electromagnetic spectral function in pion matter

We are now in position to discuss our numerical results, starting with the in-medium  $\rho$  self-energy in Sec. 5.1, followed by the EM spectral function in Sec. 5.2 and the temperature dependence of the electric conductivity in Sec. 5.3.

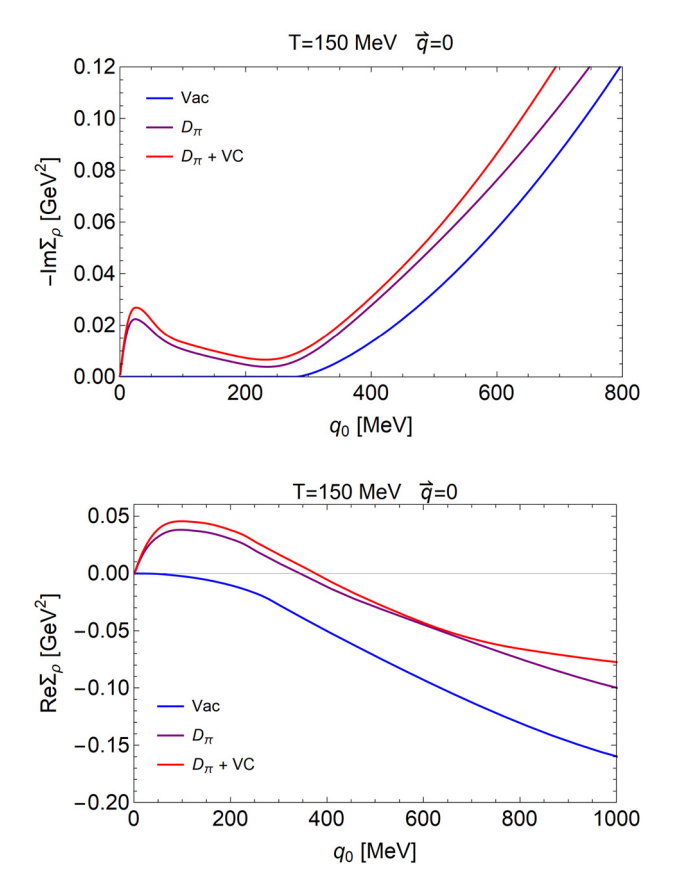


Fig. 10. Imaginary (upper panel) and real part (lower panel) of the transverse projection of the  $\rho$  self-energy in vacuum (blue line) and at T=150 MeV with (purple) and without vertex corrections (red). The results include both  $\rho$  and  $\sigma$  resonances in the  $\pi\pi$  scattering amplitude.

### 5.1. Rho self-energy

Let us first illustrate the role of the vertex corrections. In Fig. 10 we display the imaginary and real parts of the transverse projection of the  $\rho$  self-energy at  $\vec{q}=0$ , with and without vertex corrections, at a temperature of T=150 MeV. Compared to the vacuum result, the use of inmedium pion propagators enhances the imaginary part considerably, most notably below the two-pion threshold where the vacuum result vanishes. At the same time the magnitude of the real part reduces, except below threshold, where the vacuum result is small and attractive while the in-medium one has turned significantly repulsive. The inclusion of vertex corrections increases the imaginary part, which is expected as they create additional inelastic channels, again most notably in the sub-threshold region, while the real part also shows a slight increase. Next, we turn to the temperature dependence of the  $\rho$  self-energy, illustrated in Fig. 11 (which includes vertex corrections). As we have seen before, the medium effects on Re $\Sigma_{\rho}^{T}$  are repulsive, causing the rho mass to increase. The increase of Im $\Sigma_{\rho}^{T}$  with temperature is again most pronounced in the low-energy regime, while the increase at higher energies produces a broadening of the  $\rho$  resonance peak. In particular, the Landau cut of the  $\rho$  self-energy, corresponding to  $\pi + \rho \to \pi$ 

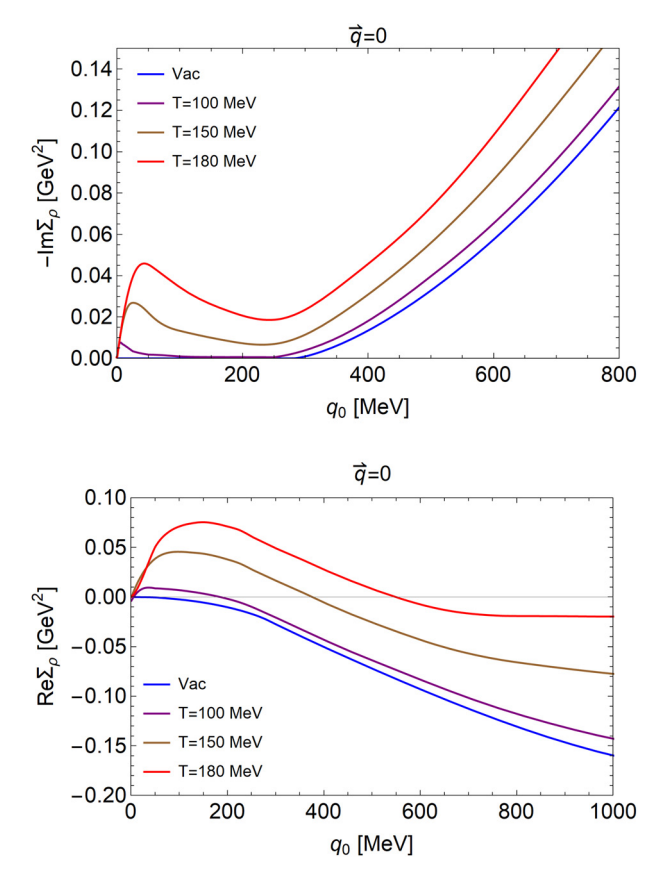


Fig. 11. Imaginary (upper panel) and real (lower panel) part of the transverse projection of the  $\rho$  self-energy at  $\vec{q}=0$  in vacuum (blue), and for various temperatures (T=100 MeV: purple, T=150 MeV: brown, and T=180 MeV: red), including vertex corrections. Results include the  $\rho$  and  $\sigma$  resonances in the  $\pi\pi$  scattering amplitude.

scattering, generates a marked bump at very low energy, which, as we will see more clearly in the next section, corresponds to a broadening of the transport peak in  $\rho_{EM}$ .

#### 5.2. EM spectral function

In this section we will discuss our results for the EM spectral function, averaged over transverse polarization and divided by energy with a normalization that yields the value of the electric conductivity at the intercept at zero energy,  $e^2\rho_{\rm EM}^{ii}/6q_0$ , recall Eq. (2). In particular, the division by energy will clearly exhibit the transport peak near vanishing energy.

We start by analyzing the different contributions from thermal  $\pi\pi$  scattering, first focusing on the case without vertex corrections at a fixed temperature of T=150 MeV, cf. Fig. 12. Maybe somewhat surprisingly, at high energies, where the unitarity cut dominates, the rescattering contributions encoded in the pion self-energy have rather little impact on the medium effects on the  $\rho$ -meson resonance peak; its thermal broadening is almost entirely driven by the Bose enhancement of the intermediate pions in the pion gas; it also features a thermal mass shift that is probably a bit too large since our  $\pi$ - $\rho$  Lagrangian is not chirally symmetric (and therefore miss-

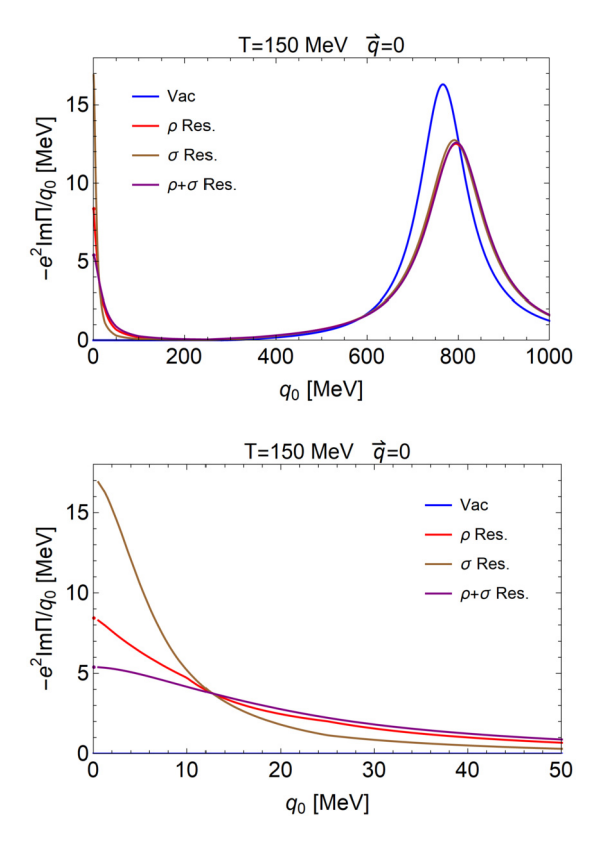


Fig. 12. Electromagnetic spectral function, scaled such that the zero-energy intercept corresponds to  $\sigma_{\rm el}$ , plotted as a function of energy at  $\vec{q}=0$  (upper and lower panels differ by the selected energy range). Results are shown excluding vertex corrections for only *P*-wave scattering (red lines), only *S*-wave scattering (brown lines), and allowing *P*- and *S*-wave scattering (purple lines), and compared to the vacuum curve (blue line).

ing, e.g., an attractive contribution from  $\rho + \pi \rightarrow a_1$  scattering; the simultaneous implementation of chiral symmetry and gauge invariance is beyond the scope of this work). In the low-energy region we now clearly see the development of the transport peak, essentially generated by the Landau cut. The pion width generated by scattering off thermal pions plays a key role, with the  $\rho$  resonance providing the dominant contribution: when only including the  $\rho$  contribution, the transport peak is much broader and the conductivity is about a factor 2 smaller compared to the case with only the  $\sigma$  contribution.

Turning to the temperature dependence, but still without vertex corrections, the  $\rho$  resonance peak shows the expected broadening increasing with temperature, cf. Fig. 13. At low energies, the conductivity decreases significantly from T=100 MeV to 150 MeV, but is almost unchanged between 150 and 180 MeV. This shows that a minimum can develop in the conductivity, caused by a misalignment of thermal pion energies with that of the resonant particles towards higher temperatures; in other words, if the thermal energies of the charge carriers are beyond those needed for resonance excitations, charge can be transported more freely again.

Finally, Fig. 14 displays the EM spectral function when vertex corrections are included, for various temperatures. The vertex corrections result in a broadening of the  $\rho$  peak that increases with temperature. This is expected because the corrections increase the  $\rho$ 's interaction with the

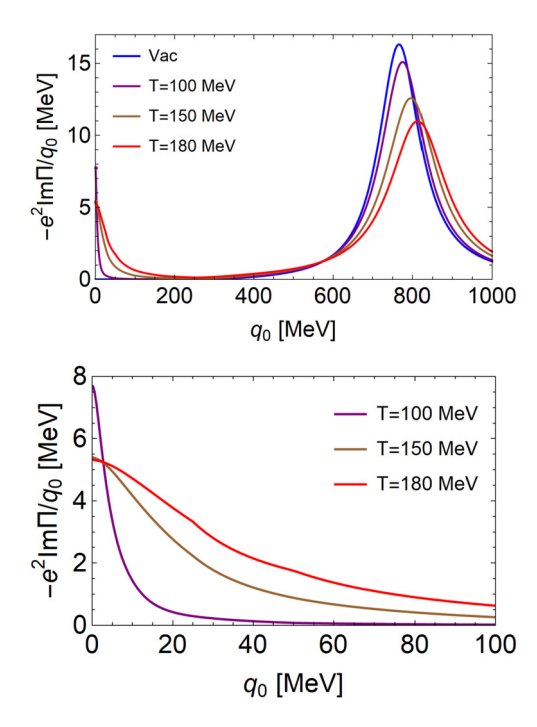


Fig. 13. Electromagnetic spectral function, scaled such that the zero-energy intercept corresponds to  $\sigma_{\rm el}$ , plotted as a function of energy at  $\vec{q}=0$  (upper and lower panels differ by the selected energy range). Results excluding vertex corrections are plotted for vacuum (blue line), at T=100 MeV (purple lines), T=150 MeV (brown lines), and T=180 MeV (red lines).

medium. Furthermore, we see an increase of the transport peak due to the vertex corrections. This is somewhat counter-intuitive, because the transport peak is proportional to the electric conductivity. Therefore, it appears that increasing the medium interaction by including vertex corrections has resulted in a more conductive medium. In order to understand this phenomenon, we note that the  $\rho$  meson does not transmit electric charge through the medium. Charge is transmitted by the charged pion states, and any increase in  $\text{Im}\Sigma_{\pi}$  will reduce the conductivity. On the other hand, the  $\rho$  self-energy determines how the external photon couples to the medium. Therefore, the various  $\rho$  self-energy diagrams represent different channels through which electric charge can travel, *i.e.*, the vertex corrections introduce additional channels, increasing the electric conductivity.

### 5.3. Electric conductivity over temperature

Let us first summarize in Fig. 15 our pion gas results for the conductivity, divided by temperature, for various scenarios as a function of temperature. When only including P-wave ( $\rho$ -resonance) scattering for the pion self-energies the temperature dependence is most pronounced, indicating that with increasing temperature the typical thermal pion energies provide markedly increasing overlap for resonance formation, thus reducing the conductivity; vertex corrections have little impact on this result. On the other, the temperature dependence is much less pronounced when only the much broader  $\sigma$  resonance is included. The pertinent conductivity is actually smaller than for  $\rho$  resonance reactions only, since the relative low thermal energies at

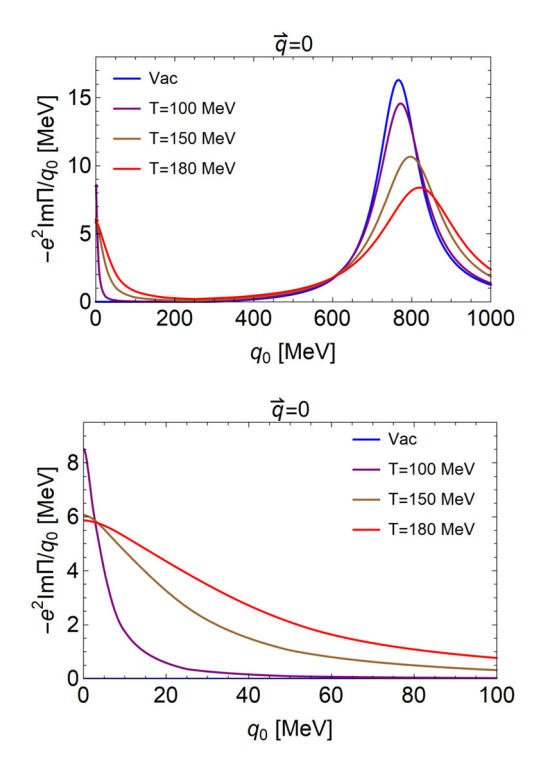


Fig. 14. Electromagnetic spectral function, scaled such that the zero-energy intercept corresponds to  $\sigma_{el}$ , plotted as a function of energy at  $\vec{q}=0$  (upper and lower panels differ by the selected energy range). We plot results including vertex corrections for T=100 MeV (purple lines), T=150 MeV (brown lines), and T=180 MeV (red lines). The vacuum line is also plotted in blue.

small temperatures are dominated by S-wave interactions; however, around  $T\gtrsim 110$  MeV, the  $\rho$  resonance interactions take over and dominate at still higher T. Interestingly, the vertex corrections have a larger effect in the  $\sigma$  channels, caused primarily by  $\Gamma_{\mu\,ab3}^{(3)C\sigma}$  (expressions are given in Appendix A). When both resonances are included, the effect of this correction is greatly reduced, because the dominant  $\rho$  self-energy diagram from  $\Gamma_{\mu\,ab3}^{(3)C\sigma}$  is inversely proportional to the pion width squared, and the  $\rho$  resonance significantly increases the pion width. At the same time, other  $\rho$  self-energy diagrams are only suppressed by the inverse pion width. In particular, the largest corrections to the  $\rho$  self-energy, when both resonances are included, turn out to arise from  $\Gamma_{\mu\nu\,ab33}^{(3)E\rho}$  and  $\Gamma_{\mu\nu\,ab33}^{(3)E\sigma}$  (see Appendix A for the explicit expressions), accounting for about 70% of the vertex corrections' contribution to the  $\rho$  self-energy. Overall, with both resonances included, the vertex corrections increase the conductivity by approximately 10% throughout.

Next, we examine the impact of the additional vertex corrections induced by the form factors. The conductivity with and without these corrections is plotted in Fig. 16, along with the conductivity without any vertex corrections. Form factors are still included in all results, in order to ensure convergence of the calculation. One can see that the form factor correction terms provide only a small increase in the total conductivity, of approximately 2.5%.

Finally, we compare our results for the hot pion matter conductivity to results from the literature in Fig. 17. Our conductivity is significantly larger than the results from kinetic theory using Breit-Wigner cross sections [8], chiral perturbation theory [10], and a relaxation time approxima-

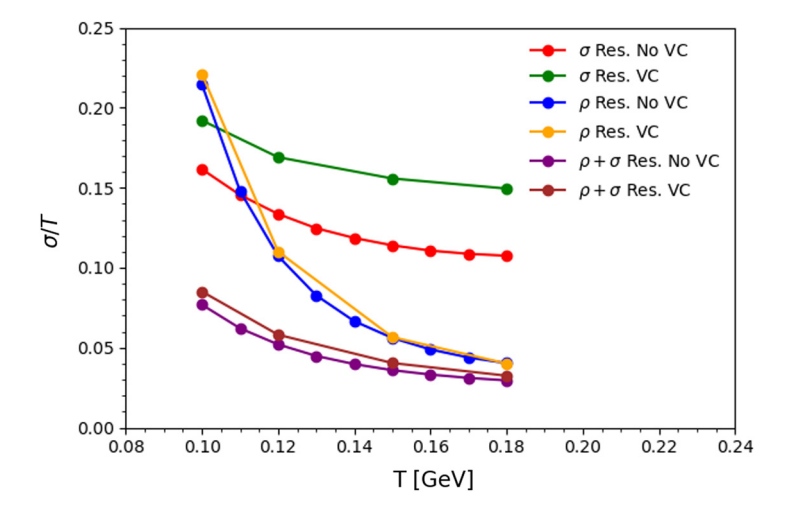


Fig. 15. Pion gas conductivity over temperature for different  $\pi\pi$  scattering resonances, with and without vertex corrections. Results including only the  $\sigma$  resonance are plotted in red (vertex corrections excluded) and green (vertex corrections included). Results including only the  $\rho$  resonance are plotted in blue (vertex corrections excluded) and orange (vertex corrections included). Results including both resonances are plotted in purple (vertex corrections excluded) and brown (vertex corrections included).

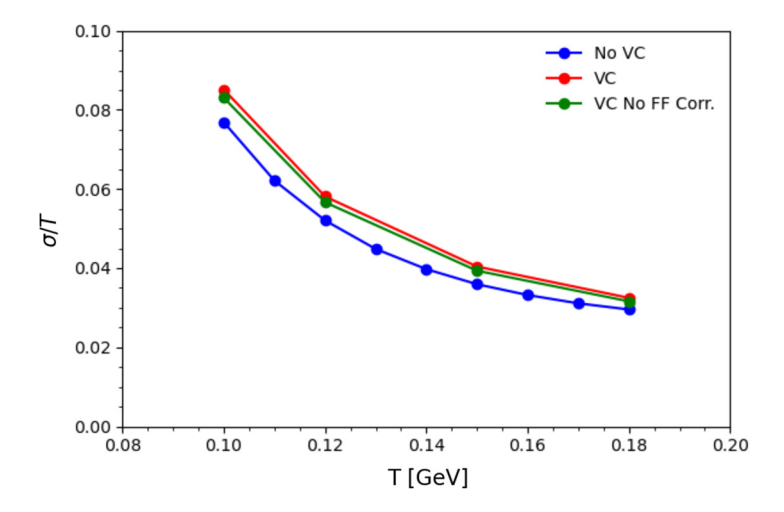


Fig. 16. Pion gas conductivity over temperature without vertex corrections (blue), with vertex corrections (red), and including all vertex corrections except those induced by the form factor (green). The results include  $\pi\pi$  scattering through rho and sigma resonances.

tion [18], but it is smaller than the K-matrix results of Ref. [16]. However, our calculation agrees well with the real-time field theory results of Ref. [17]. In Refs. [8,10,16,17] expressions for the conductivity are provided in terms of either the pion width or the relaxation time (sometimes equated to the collisions time), which are similar to our Eq. (27); however, the inputs for the pion width vary considerably. For example, in Ref. [18], the momentum averaged charged-pion relaxation time at T=150 MeV (using vacuum  $\rho$  and  $\sigma$  channel cross sections) amounts to ca. 2 fm/c (3 fm/c for neutral pions), which translates into a reaction rate of  $\sim$ 100 MeV, substantially

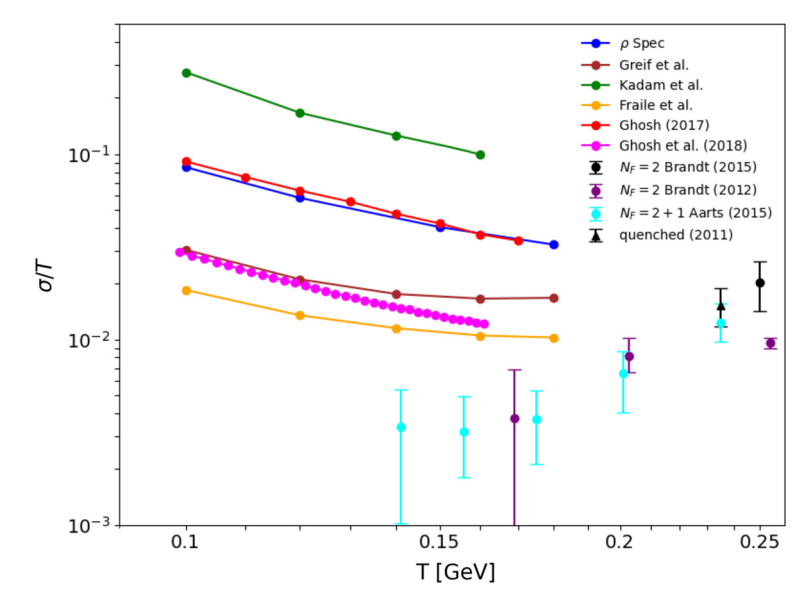


Fig. 17. Our results for the electric conductivity over temperature (blue line) compared to previous calculations in pion matter and IQCD results: brown line: kinetic-theory using Breit-Wigner cross sections [8], green line: K-matrix approach [16], orange line: chiral perturbation theory [10], red line: real-time thermal field theory [17], magenta line: relaxation time approximation with Chapman-Enskog technique [18], black, purple and cyan dots: lattice QCD for  $N_f$ =2 light flavors [13,14] and for  $N_f$ =2+1 [12], respectively. The black dashed line indicates a proposed lower bound from Ref. [9] using a holographic calculation for a supersymmetric Yang-Millls plasma.

larger than our optical potential of  $\Gamma=-2\mathrm{Im}U_\pi\simeq 20-30$  MeV. Fig. 17 also indicates that the pion gas results are significantly larger than IQCD calculations, with most IQCD results falling below a proposed lower bound from a calculation for a strongly coupled supersymmetric Yang-Mills plasma using AdS/CFT duality [9] (which, however, depends on the number of degrees of freedom in the calculation and therefore may not be appropriate to be compared to pion matter; we will return to this issue Sec. 6.1 below). Furthermore, in Ref. [12] it is cautioned that the extraction of the conductivity at low temperature from IQCD computations of Euclidean vector-current correlators faces difficulties in extracting narrow transport peaks created by hadronic interactions.

Our results support a pion matter conductivity significantly higher than the lower bound proposed in Ref. [9]. Furthermore, our calculations indicate that the effects of the vertex corrections are rather small (at the  $\sim 10\%$  level), whereas the conductivity is dominated by the Landau cut of the  $\rho$  self-energy, which is related to the pion's collisional width. As demonstrated in Eq. (27), consistent with kinetic theory, the conductivity is essentially inversely proportional to the pion's width. Therefore, the conductivity is sensitive to pionic interactions and a robust calculation of the pion's width is required in order to reliably extract the conductivity.

### 6. Applications of the electromagnetic spectral function

In this section we further analyze the EM spectral function by utilizing it to calculate the charge susceptibility which facilitates a more quantitative context for comparisons to conjectured quantum lower bound, and testing our calculation's with a current conservation sum rule.

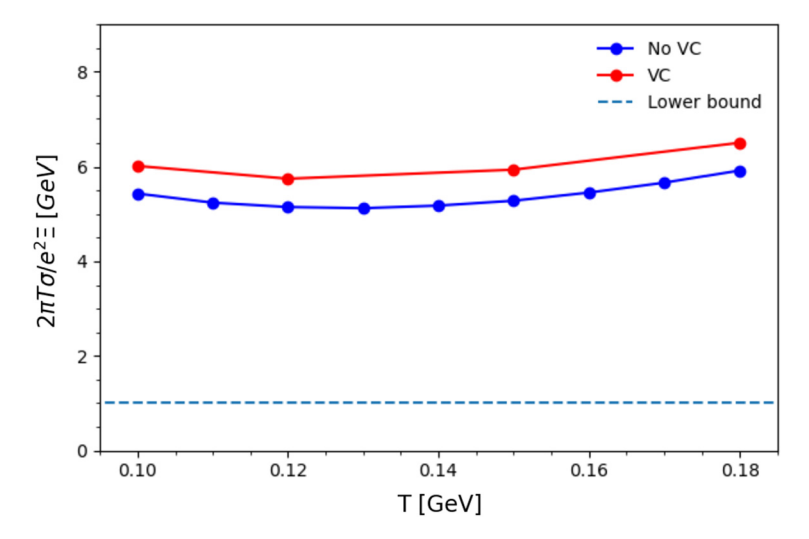


Fig. 18. Electric conductivity divided by  $e^2$  times the charge susceptibility, normalized such that the lower bound is one. The susceptibility is calculated without vertex corrections, but results are shown for the conductivity with (red line) and without (blue line) vertex corrections and compared to the lower bound calculated in Ref. [9] (black dashed line).

### 6.1. Charge susceptibility

When comparing  $\sigma_{\rm el}/T$  to proposed quantum lower bounds (and lQCD calculations), some care is in order as this quantity, albeit dimensionless, depends on the number of degrees of freedom in the theory, which is quite different for a pion gas. To mitigate this difference, it has been proposed [9] to rather divide the conductivity by the charge susceptibility. To leading order in  $e^2$  the susceptibility is related to the EM Debye mass squared [41–44]. Within the VDM one can express the Debye mass in terms of the temporal component of the  $\rho$  propagator [45],

$$\Xi = m_D^2 = -\lim_{\vec{q} \to 0} \left[ (m_\rho^0)^4 / g_\rho^2 D_\rho^{00} (q_0 = 0, \vec{q}) - (m_\rho^0)^4 / g_\rho^2 D_{\rho \, vac}^{00} (0, 0) \right]. \tag{57}$$

We recall that the conductivity corresponds to the time-like limit of  ${\rm Im}\Pi^{\mu\nu}_{\rm EM}$ , while the susceptibility is determined by the space-like limit of  ${\rm Re}\Pi^{\mu\nu}_{\rm EM}$ . Though our formalism can be extended to finite  $\vec q$ , we have not calculated vertex corrections at finite  $\vec q$  yet, as this presents significant numerical challenges while only producing a  $\sim\!10\%$  effect. Therefore, we here extract  $\Xi$  using from  $\rho$  self-energy in  $\Pi^{00}_{\rm EM}$  with dressed pion propagators neglecting vertex corrections.

In Fig. 18 we plot our result for  $(2\pi T\sigma_{\rm el})/(e^2\Xi)$  and compare it to the proposed lower bound of 1 from Ref. [9]. We see that our pion-gas values are approximately a factor of five larger than this lower bound. Furthermore, our results display a minimum between 120 and 140 MeV. Therefore, we see that even when the number of degrees of freedom is accounted for, our result is well above the proposed lower bound.

#### 6.2. Current conservation sum rule

As a further test of the internal consistency of our calculation, we insert our EM spectral function into a sum rule derived based on charge conservation in Ref. [46],

Violation of the sum rule proposed in ref. [46] for various temperatures.				
Calc	100 MeV	120 MeV	150 MeV	180 MeV
No VC	.32%	.34%	.36%	.57%
VC	.92%	.67%	.33%	.24%

.39%

.32%

.35%

Table 1 Violation of the sum rule proposed in ref. [46] for various temperatures.

.38%

$$\int_{0}^{\infty} dw \frac{1}{w} \operatorname{Im}\Pi(w, T) = \int_{0}^{\infty} dw \frac{1}{w} \operatorname{Im}\Pi_{vac}(w) . \tag{58}$$

In order to quantify the violation of the sum rule, we calculate the percent change of the left-hand side of Eq. (58) relative to the vacuum value. The violations with and without vertex correction are collected in Table 1. Before including vertex corrections the violation is on average less than 0.5%. When vertex corrections are included the violation increases for T=100 MeV and 120 MeV, but is reduced for T=150 MeV and 180 MeV. Furthermore, adding the corrections induced by the form factors tends to increase the violation. While this increase provides further motivation to investigate a form factor that improves on gauge invariance, it is reassuring that the violation is consistently less than 1%. In order to gain precision at this level we would likely also have to refine the numerical computations and calculate further iterations of the self-consistency equation induced by the pion self-energy.

### 7. Summary and future work

VC No FF Corr.

We have calculated the electric conductivity of hot pion matter employing a quantum-field theoretic approach that is rooted in successful descriptions of thermal-dilepton spectra in heavyion collisions [1,47]. Based on the VDM, the EM spectral function is related to the imaginary part of the light vector-meson propagators (most notably the  $\rho$ ), and interactions with the thermal medium have been evaluated through the  $\rho$  self-energy. In pion matter the latter exhibits a transport peak through its Landau cut which corresponds to the scattering of a low-energy  $\rho$  (or photon) with thermal pions from the heat bath. The width of the transport peak (and with it a finite conductivity) is generated through thermal  $\pi\pi$  scattering producing finite collisional widths for both in- and outgoing pions. We have included S- and P-wave scatterings through  $\sigma$  and  $\rho$ resonances, respectively, to obtain in-medium pion self-energies and resummed those through the pion propagators within the  $\rho$  self-energy. We then remedied violations of gauge invariance induced by this dressing with suitably constructed corrections to the  $\rho\pi\pi$  and  $\rho\rho\pi\pi$  vertices guided by Ward-Takahashi identities. The effect of the vertex corrections on the conductivity turns out to be rather moderate, resulting in an approximately 10% increase due to additional charge-conduction channels provided by the modified vertices. Both S- and P-wave  $\pi\pi$  scattering contribute to the conductivity, with the latter (former) being the leading contribution at temperatures above (below)  $\sim 100$  MeV.

Our results suggest a conductivity significantly larger than found in previous calculations using kinetic theory, chiral perturbation theory, a Chapman-Enskog type relaxation time approximation, or a K-matrix formalism [8,10,16,18]. Our values agree with the real-time field theory calculation in Ref. [17]. However, the variation in the conductivity does not appear to be due to the choice of formalism, as the different formalisms produce similar expressions for the conductivity in terms of the pion width. Rather, the most important differences appear to originate

from the model for the in-medium self-energy. Furthermore, our conductivity is well above the quantum lower bound proposed in Ref. [9]. This can be better quantified when normalizing the  $\sigma_{el}$  values by the pertinent charge susceptibilities, as to remove the dependency on the number of degrees of freedom in the different systems. In that normalization our result is about a factor of  $\sim$ 5 above the lower bound.

We intend to extend our formalism to study the strong-coupling limit by increasing  $g_{\rho}$ , as our calculations, rooted in quantum mechanics, may be expected to respect a pertinent lower bound. In this limit, the higher-order corrections may not be as heavily suppressed, therefore they will require further scrutiny. Another extension concerns the inclusion of additional hadronic species in the confined medium. This will require a more complete calculation of the in medium  $\rho$  selfenergy, for which existing results can be utilized [1]. In particular, we will include baryonic effects on the self-energy, which will be crucial when comparing our calculation to results from HICs. The effect of nucleons at finite density and temperature can be included by combining this work's pion self-energy with that of Ref. [26] while accounting for additional vertex corrections to the  $\rho$  self-energy. Furthermore, we will include direct couplings of the  $\rho$  to mesons and baryons in the surrounding hot hadronic medium which are usually dominated by resonance excitations. Both the probing of the strong-coupling limit and the more complete hadronic matter calculation will likely bring the conductivity closer to the lower bound. Furthermore, in a more strongly coupled medium an increase in the conductivity due to the vertex corrections may also occur and provide a significant contribution. This may be one of the mechanisms that may contribute to a saturation value within a quantum-mechanical framework with conserving approximations, and thus enable to probe quantum lower bounds in a controlled way. Finally, experimental efforts to measure very-low mass dileptons are underway by HADES at GSI, STAR at BNL, and ALICE-3 for LHC run-5 down to a few tens of MeV [5-7]. Our calculations suggest that these measurements should be able to access the mass region where the transport peak is prevalent, and thus may provide a measurement of the conductivity. However, more quantitative predictions of thermal-emission spectra from heavy-ion collisions in the very-low-mass region require a more complete hadronic matter calculation, as indicated above.

### **Declaration of competing interest**

The authors declare that they have no known competing financial interests or personal relationships that could have appeared to influence the work reported in this paper.

### Data availability

Data will be made available on request.

### Acknowledgements

This work has been supported by the U.S. National Science Foundation under grants PHY-1913286 and PHY-2209335.

### Appendix A. Vertex correction formulation

In this appendix we elaborate on our calculation of the vertex corrections. We give the explicit expressions for the vertex corrections in Sec. A.1, implement form factors in Sec. A.2, and discuss the elimination of double-counting issues from the  $\rho$  self-energy in Sec. A.3.

#### A.1. Vertex correction integrals

The corrections to the  $\rho\pi\pi$  vertex due to the  $\rho$  resonance are given by

$$\Gamma_{\mu \, ab3}^{(3)A\rho}(k,q) = \epsilon_{3ab} \frac{3g_{\rho}^{3}}{2} T \sum_{n(even)} \int \frac{d^{3}p}{(2\pi)^{3}} \left[ D_{\pi}(p) D_{\rho}^{\nu\lambda}(k+p) g_{\mu\lambda}(k-p)_{\nu} \right] \\
\times FF_{\rho}[p,k] FF_{\rho}[q+p,-q+k] \Big]_{p_{0}=iw_{n}}, \qquad (A.1)$$

$$\Gamma_{\mu \, ab3}^{(3)B\rho}(k,q) = \epsilon_{3ab} \frac{3g_{\rho}^{3}}{2} T \sum_{n(even)} \int \frac{d^{3}p}{(2\pi)^{3}} \left[ D_{\pi}(p) D_{\rho}^{\nu\lambda}(q+k+p) g_{\mu\lambda}(q+k-p)_{\nu} \right] \\
\times FF_{\rho}[p,q+k] FF_{\rho}[q+p,k] \Big]_{p_{0}=iw_{n}}, \qquad (A.2)$$

$$\Gamma_{\mu \, ab3}^{(3)C\rho}(k,q) = \epsilon_{3ab} \frac{g_{\rho}^{3}}{2} T \sum_{n(even)} \int \frac{d^{3}p}{(2\pi)^{3}} \left[ D_{\pi}(p) D_{\pi}(q+p) D_{\rho}^{\nu\lambda}(q+k+p) (2p+q)_{\mu} \right] \\
\times (-p+k+q)_{\lambda}(k-p-q)_{\nu} FF_{\rho}[p,q+k] FF_{\rho}[q+p,k] \Big]_{p_{0}=iw_{n}}. \qquad (A.3)$$

The corrections to the  $\rho\pi\pi$  vertex due to the  $\sigma$  resonance are given by

$$\Gamma_{\mu ab3}^{(3)C\sigma}(k,q) = \epsilon_{3ab} \frac{g_{\rho} g_{\sigma}^{2}}{2} T \sum_{n(even)} \int \frac{d^{3}p}{(2\pi)^{3}} \left[ D_{\pi}(p) D_{\pi}(q+p) D_{\sigma}(q+k+p) \right] \times ((q+k+p)^{2} - m_{\pi}^{2}) (2p+q)_{\mu} FF_{\rho}[p,q+k] FF_{\rho}[q+p,k]$$

$$(A.4)$$

The corrections to the  $\rho\rho\pi\pi$  vertex due to the  $\rho$  resonance are given by

$$\Gamma_{\mu\nu\,ab33}^{(4)A\rho}(k,q) = (5\delta_{ab} - 3\delta_{3a}\delta_{3b}) \frac{ig_{\rho}^{4}}{2} T \sum_{n(even)} \left[ \int \frac{d^{3}p}{(2\pi)^{3}} D_{\pi}(p) D_{\rho}^{\mu\nu}(q+k+p) \right] \times FF_{\rho}[q+p,k]^{2} + (k \to -k),$$

$$\Gamma_{\mu\nu\,ab33}^{(4)B_{1}\rho}(k,q) = -2\delta_{ab} \frac{ig_{\rho}^{4}}{2} T \sum_{n(even)} \left[ \int \frac{d^{3}p}{(2\pi)^{3}} D_{\pi}(p) D_{\pi}(p+q) D_{\rho\nu\beta}(k+p) \right] \times (2p+q)_{\mu}(p-k)^{\beta} FF_{\rho}[p,k]^{2} \Big]_{p_{0}=iw_{n}} + (k \to -k),$$
(A.6)

$$\Gamma_{\mu\nu ab33}^{(4)B_{2}\rho}(k,q) = \Gamma_{\nu\mu ab}^{(4)B_{1}\rho}(k,q), \tag{A.7}$$

$$\Gamma_{\mu\nu ab33}^{(4)E\rho}(k,q) = (\delta_{ab} + \delta_{3a}\delta_{3b}) \frac{ig_{\rho}^{4}}{2} T \sum_{n(even)} \left[ \int \frac{d^{3}p}{(2\pi)^{3}} D_{\pi}(p)^{2} D_{\pi}(p+q) D_{\rho}(k+p)_{\alpha\beta} \right] \times (2p+q)_{\mu}(p-k)^{\alpha}(p-k)^{\beta}(2p+q)_{\nu} FF_{\rho}[p,k]^{2}$$

$$+ (k \to -k), \tag{A.8}$$

$$\Gamma_{\mu\nu ab33}^{(4)G\rho}(k,q) = -2(\delta_{3a}\delta_{3b} + \delta_{ab}) \frac{ig_{\rho}^{4}}{2} T \sum_{n(even)} \left[ \int \frac{d^{3}p}{(2\pi)^{3}} D_{\pi}(p)^{2} D_{\rho}^{\alpha\beta} \right] \times (k+p)(k-p)_{\alpha}(k-p)_{\beta} g_{\mu\nu} FF_{\rho}[p,k]^{2}$$

$$\times (k+p)(k-p)_{\alpha}(k-p)_{\beta} g_{\mu\nu} FF_{\rho}[p,k]^{2}$$

$$(A.9)$$

Finally the corrections to the  $\rho\rho\pi\pi$  vertex due to the  $\sigma$  resonance are given by

$$\Gamma_{\mu\nu\,ab33}^{(4)E\sigma}(k,q) = (\delta_{ab} - \delta_{3a}\delta_{3b}) \frac{ig_{\rho}^{2}g_{\sigma}^{2}}{2} T \sum_{n(even)} \left[ \int \frac{d^{3}p}{(2\pi)^{3}} D_{\pi}(p)^{2} D_{\pi}(p+q) D_{\sigma}(k+p) \right] \times ((k+p)^{2} - m_{\pi}^{2}) (2p+q)_{\mu} (2p+q)_{\nu} FF_{\sigma}[p,k]^{2} \Big]_{p_{0}=iw_{n}} + (k \to -k),$$

$$\Gamma_{\mu\nu\,ab33}^{(4)G\sigma}(k,q) = 2(\delta_{3a}\delta_{3b} - \delta_{ab}) \frac{ig_{\rho}^{2}g_{\sigma}^{2}}{2} T \sum_{n(even)} \left[ \int \frac{d^{3}p}{(2\pi)^{3}} D_{\pi}(p)^{2} D_{\sigma}(k+p) \right] \times ((k+p)^{2} - m_{\pi}^{2}) g_{\mu\nu} FF_{\sigma}[p,k]^{2} \Big]_{p_{0}=iw_{n}},$$
(A.11)

where we have excluded all corrections including  $\rho\rho\rho$  or  $\rho\rho\rho\rho$  vertices.

### A.2. Vertex correction form factor correction

Here we give the expressions for the total regularized vertex corrections, including terms where the  $\rho$  meson couples to a heavy-pion propagator.

$$\begin{split} \Gamma_{\mu ab3}^{\prime(3)}(k,q) &= \Gamma_{\mu ab3}^{(3)\rho}(k,q) + \Gamma_{\mu ab3}^{(3)\sigma}(k,q) \\ &+ g_{\rho} \epsilon_{3ab} (2k+q)_{i} \Big( \frac{\Sigma_{\pi}^{(\rho)}(q+k)}{A_{\rho}^{2} + \vec{k}^{2}} + \frac{\Sigma_{\pi}^{(\rho)}(k)}{A_{\rho}^{2} + (\vec{q} + \vec{k})^{2}} \Big) \\ &+ g_{\rho} \epsilon_{3ab} (2k+q)_{i} \Big( \frac{\Sigma_{\pi}^{(\sigma)}(q+k)}{A_{\sigma}^{2} + \vec{k}^{2}} + \frac{\Sigma_{\pi}^{(\sigma)}(k)}{A_{\sigma}^{2} + (\vec{q} + \vec{k})^{2}} \Big), \end{split} \tag{A.12}$$
 
$$\Gamma_{\mu\nu ab33}^{\prime(4)}(k,q) = \Gamma_{\mu\nu ab33}^{(4)\rho}(k,q) + \Gamma_{\mu\nu ab33}^{(4)\sigma}(k,q) \\ &- \frac{ig_{\rho} \epsilon_{3ca}}{A_{\rho}^{2} + \vec{k}^{2}} \Big[ (2k-q)_{i} \Gamma_{\nu bc3}^{(3)\rho}(k,-q) + (2k+q)_{j} \Gamma_{\mu cb3}^{(3)\rho}(-q-k,q) \Big] \\ &- \frac{ig_{\rho} \epsilon_{3ca}}{A_{\sigma}^{2} + \vec{k}^{2}} \Big[ (2k-q)_{i} \Gamma_{\nu bc3}^{(3)\sigma}(k,-q) + (2k+q)_{j} \Gamma_{\mu cb3}^{(3)\sigma}(-q-k,q) \Big] \end{split}$$

$$-\frac{ig_{\rho}\epsilon_{3bc}}{A_{\rho}^{2}+\vec{k}^{2}}\left[(2k+q)_{i}\Gamma_{vac3}^{(3)\rho}(-k,-q)+(2k-q)_{j}\Gamma_{\mu ca3}^{(3)\rho}(-q+k,q)\right]$$

$$-\frac{ig_{\rho}\epsilon_{3bc}}{A_{\sigma}^{2}+\vec{k}^{2}}\left[(2k+q)_{i}\Gamma_{vac3}^{(3)\sigma}(-k,-q)+(2k-q)_{j}\Gamma_{\mu ca3}^{(3)\sigma}(-q+k,q)\right]$$

$$-ig_{\rho}^{2}(\delta_{ab}-\delta_{3a}\delta_{3b})\left\{(2k-q)_{i}(2k-q)_{j}\left[\frac{\Sigma_{\pi}^{(\rho)}(-q+k)}{(A_{\rho}^{2}+\vec{k}^{2})^{2}}\right]\right.$$

$$+\frac{2\Sigma_{\pi}^{(\rho)}(k)}{(A_{\rho}^{2}+(-\vec{q}+\vec{k})^{2})(A_{\rho}^{2}+\vec{k}^{2})}+\frac{\Sigma_{\pi}^{(\sigma)}(-q+k)}{(A_{\sigma}^{2}+\vec{k}^{2})^{2}}$$

$$+\frac{2\Sigma_{\pi}^{(\sigma)}(k)}{(A_{\sigma}^{2}+(-\vec{q}+\vec{k})^{2})(A_{\sigma}^{2}+\vec{k}^{2})}\right]+(2k+q)_{i}(2k+q)_{j}\left[\frac{\Sigma_{\pi}^{(\rho)}(q+k)}{(A_{\rho}^{2}+\vec{k}^{2})^{2}}\right]$$

$$+\frac{2\Sigma_{\pi}^{(\rho)}(k)}{(A_{\rho}^{2}+(\vec{q}+\vec{k})^{2})(A_{\rho}^{2}+\vec{k}^{2})}+\frac{\Sigma_{\pi}^{(\sigma)}(q+k)}{(A_{\sigma}^{2}+\vec{k}^{2})^{2}}$$

$$+\frac{2\Sigma_{\pi}^{(\rho)}(k)}{(A_{\rho}^{2}+(\vec{q}+\vec{k})^{2})(A_{\rho}^{2}+\vec{k}^{2})}-4\delta_{ij}\frac{\Sigma_{\pi}^{(\rho)}(k)}{A_{\rho}^{2}+\vec{k}^{2}}-4\delta_{ij}\frac{\Sigma_{\pi}^{(\sigma)}(k)}{A_{\sigma}^{2}+\vec{k}^{2}}\right\},$$

$$(A.13)$$

where  $\Gamma^{(3)(\rho/\sigma)}_{\mu\,ab3}$  and  $\Gamma^{(4)(\rho/\sigma)}_{\mu\nu\,ab33}$  are the total regularized vertex corrections,  $A_R=\sqrt{\Lambda_R^2/4+m_\pi^2}$ , and the indices i and j designate the spatial components of  $\mu$  and  $\nu$ . For i=0 or j=0 the corresponding term should be dropped.

#### A.3. Removing double counting

We must take care to avoid double-counting of self-energy diagrams when calculating  $\Sigma_{\rho}^{\mu\nu}$ . Double-counting occurs due to the self-consistent treatment of the  $\rho\pi\pi$  vertex and the pion propagator. For the corrections to the  $\rho\pi\pi$  vertex, double-counting is encountered due to the presence of the Landau cut within vertex corrections, *i.e.*, thermal  $\pi\pi$  scattering with the external  $\rho$ . Furthermore, double-counting is generated in all the corrections to the  $\rho\rho\pi\pi$  vertex.

For the corrections to the  $\rho\pi\pi$  vertex, double-counting occurs due to  $\Gamma^{(3)C\rho}_{\mu\,ab3}$  and  $\Gamma^{(3)C\sigma}_{\mu\,ab3}$ . We see that these vertex corrections produce the same self-energy diagram when used to dress the right or left hand vertex of the  $\pi\pi$ -loop. Furthermore, consider the higher-order corrections obtained by dressing  $\Gamma^{(3)C\rho}_{\mu\,ab3}$  or  $\Gamma^{(3)C\sigma}_{\mu\,ab3}$  with three-point vertex corrections. Such higher-order vertex corrections do not produce unique contributions to the  $\rho$  self-energy, because these self-energies are also produced by dressing one vertex of the  $\pi\pi$ -loop with  $\Gamma^{(3)C\rho}_{\mu\,ab3}$  or  $\Gamma^{(3)C\sigma}_{\mu\,ab3}$  and the other vertex with a three-point vertex correction. Double-counting is encountered because the thermal particles in the vertex corrections are identical to those in the  $\rho$  self-energy. The vertex corrections are defined such that they do not include vacuum particles, therefore we only encounter double-counting when dressing the Landau cut of  $\Sigma^{\mu\nu}_{\rho}$ . In this work we avoid double-counting in the  $\pi\pi$ -loop by only dressing the right-hand  $\rho\pi\pi$  vertex with the self-consistently calculated  $\Gamma^{(3)C\rho}_{\mu\,ab3}$  or  $\Gamma^{(3)C\sigma}_{\mu\,ab3}$  vertex correction.

Next, we address double-counting in the corrections to the  $\rho\rho\pi\pi$  vertex. As we have seen for

Next, we address double-counting in the corrections to the  $\rho\rho\pi\pi$  vertex. As we have seen for the unitarity cut of the  $\pi\pi$ -loop, double-counting is avoided when we dress the vacuum tadpole loop and its Bose enhancement. However, when the pion in the tadpole loop is thermal, all of

the four-point corrections generate double-counting. The double counting is generated by one of two scenarios: First, the  $\rho$  self-energy contribution derived from the correction is equivalent to a self-energy obtained from dressing the  $\pi\pi$ -loop. We see that  $\Gamma^{(4)B_1\rho}_{\mu\nu ab33}$  and  $\Gamma^{(4)B_2\rho}_{\mu\nu ab33}$  can be generated by dressing the  $\pi\pi$ -loop with  $\Gamma^{(3)A\rho}_{\mu ab3}$ . Alternatively,  $\Gamma^{(4)E\rho}_{\mu\nu ab33}$ ,  $\Gamma^{(4)G\rho}_{\mu\nu ab33}$ ,  $\Gamma^{(4)E\sigma}_{\mu\nu ab33}$ , and  $\Gamma^{(4)G\rho}_{\mu\nu ab33}$  simply dress a pion propagator in  $\Sigma^{\mu\nu}_{\rho}$  with a thermal  $\pi\rho$  or  $\pi\sigma$  loop. However, these diagrams are already included in  $\Sigma^{\mu\nu}_{\rho}$  through the resummation of the pion propagator, introduced in Eq. (28). The second scenario occurs in  $\Gamma^{(4)A\rho}_{\mu\nu ab33}$ . In this case a unique diagram is generated by the vertex corrections, however, the diagram includes a  $\pi\pi$ -loop in which the two pions have identical 4-momentum. This configuration generates double-counting, because the pions are indistinguishable. Therefore, an additional symmetry factor of  $\frac{1}{2}$  needs to be added to  $\Gamma^{(4)A\rho}_{\mu\nu ab33}$  when the tadpole loop contains a thermal pion.

We have verified analytically that if all double counting is dropped gauge invariance is not violated.

### Appendix B. Matsubara sums

In this appendix we establish the spectral representations used to perform the Matsubara sums appearing in the  $\rho$  self-energy, and provide the results of the summations. We begin by presenting the corrections to the  $\pi\pi$ -loop from the three-point vertex corrections in Sec. B.1. In Sec. B.2 we present the corrections to the tadpole loop from the four-point vertex corrections, and in Sec. B.3 we give the total correction to the  $\rho$  self-energy.

### B.1. $\pi\pi$ -loop corrections

Here we write the imaginary parts of  $\Gamma^{(3)A\rho}_{\mu\,ab3}$ ,  $\Gamma^{(3)B\rho}_{\mu\,ab3}$ ,  $\Gamma^{(3)C\rho}_{\mu\,ab3}$ , and  $\Gamma^{(3)C\sigma}_{\mu\,ab3}$ , relevant for maintaining gauge invariance.

$$\begin{split} \operatorname{Im}\Gamma^{(3)A\rho}_{\mu\,ab3}(k,q) &= -\epsilon_{3ab} \frac{3g_{\rho}^{3}}{2} \int \frac{d^{3}p}{(2\pi)^{3}} \int_{0}^{\infty} \frac{dw}{-\pi} \bigg[ \operatorname{Im}[D_{\pi}(p)] \operatorname{Im}[D_{\rho}^{\nu\lambda}(p+k)] g_{\mu\lambda}(k-p)_{\nu} \\ &\times \operatorname{FF}_{\rho}[-q+p,q+k] \operatorname{FF}_{\rho}[p,k] \Theta(k_{0}+w) (f(w)-f(k_{0}+w)) \bigg]_{p_{0}=w} \\ &+ \epsilon_{3ab} \frac{3g_{\rho}^{3}}{2} \int \frac{d^{3}p}{(2\pi)^{3}} \int_{0}^{\infty} \frac{dw}{-\pi} \bigg[ \operatorname{Im}[D_{\pi}(p)] \operatorname{Im}[D_{\rho}^{\nu\lambda}(p+k)] g_{\mu\lambda}(k-p)_{\nu} \\ &\times \operatorname{FF}_{\rho}[-q+p,q+k] \operatorname{FF}_{\rho}[p,k] \Theta(-k_{0}+w) \\ &\times (f(w)-f(-k_{0}+w)) \bigg]_{p_{0}=-w}, \end{split} \tag{B.1} \\ \operatorname{Im}\Gamma^{(3)B\rho}_{\mu\,ab3}(k,q) &= -\epsilon_{3ab} \frac{3g_{\rho}^{3}}{2} \int \frac{d^{3}p}{(2\pi)^{3}} \int_{0}^{\infty} \frac{dw}{-\pi} \bigg[ \operatorname{Im}[D_{\pi}(p)] \operatorname{Im}[D_{\rho}^{\nu\lambda}(q+k+p)] \\ &g_{\mu\lambda}(q+k-p)_{\nu} \operatorname{FF}_{\rho}[q+p,k] \operatorname{FF}_{\rho}[p,q+k] \Theta(q_{0}+k_{0}+w) \\ &\times (f(w)-f(q_{0}+k_{0}+w)) \bigg]_{p_{0}=w} \end{split}$$

$$+\epsilon_{3ab} \frac{3g_{\rho}^{3}}{2} \int \frac{d^{3}p}{(2\pi)^{3}} \int_{0}^{\infty} \frac{dw}{-\pi} \left[ \text{Im}[D_{\pi}(p)] \text{Im}[D_{\rho}^{\nu\lambda}(q+k+p)] \right] \\
\times g_{\mu\lambda}(q+k-p)_{\nu} \text{FF}_{\rho}[q+p,k] \text{FF}_{\rho}[p,q+k] \Theta(-q_{0}-k_{0}+w) \\
\times (f(w)-f(-q_{0}-k_{0}+w)) \right]_{p_{0}=-w}. \tag{B.2}$$

In order to help group  $\Gamma^{(3)C\rho}_{\mu\,ab3}$  and  $\Gamma^{(3)C\sigma}_{\mu\,ab3}$  into spectral representations we break each term into four functions:

$$\begin{split} \operatorname{Im}\Gamma^{(3)C\rho k}_{\mu ab3}(k,q) &= \epsilon_{3ab} \frac{g_{\rho}^{3}}{2} \int \frac{d^{3}p}{(2\pi)^{3}} \int_{0}^{\infty} \frac{dw}{-\pi} \bigg[ \operatorname{Im}[D_{\pi}(p)] \operatorname{Re}[D_{\pi}(q-p)] \operatorname{Im}[D_{\rho}^{\nu\lambda}(p+k)] \\ &\times (-2p+q)_{\mu}(k+2q-p)_{\lambda}(k-p)_{\nu} \operatorname{FF}_{\rho}[p,k] \\ &\times \operatorname{FF}_{\rho}[-q+p,q+k] \Theta(k_{0}+w)(f(w)-f(k_{0}+w)) \bigg]_{p_{0}=w} \\ &- \epsilon_{3ab} \frac{g_{\rho}^{3}}{2} \int \frac{d^{3}p}{(2\pi)^{3}} \int_{0}^{\infty} \frac{dw}{-\pi} \bigg[ \operatorname{Im}[D_{\pi}(p)] \operatorname{Re}[D_{\pi}(q-p)] \\ &\times \operatorname{Im}[D_{\rho}^{\nu\lambda}(p+k)] (-2p+q)_{\mu}(-p+k+2q)_{\lambda}(k-p)_{\nu} \operatorname{FF}_{\rho}[p,k] \\ &\times \operatorname{FF}_{\rho}[-q+p,q+k] \Theta(-k_{0}+w)(f(w)-f(-k_{0}+w)) \bigg]_{p_{0}=-w} , \\ (B.3) \\ \operatorname{Im}\Gamma^{(3)C\rho q}_{\mu ab3}(k,q) &= \epsilon_{3ab} \frac{g_{\rho}^{3}}{2} \int \frac{d^{3}p}{(2\pi)^{3}} \int_{0}^{\infty} \frac{dw}{-\pi} \bigg[ \operatorname{Im}[D_{\pi}(p)] \operatorname{Re}[D_{\pi}(q+p)] \\ &\times \operatorname{Im}[D_{\rho}^{\nu\lambda}(q+k+p)] (-2p-q)_{\mu}(-p+k+q)_{\lambda} \\ &\times (k-q-p)_{\nu} \operatorname{FF}_{\rho}[q+p,k] \operatorname{FF}_{\rho}[p,q+k] \Theta(q_{0}+k_{0}+w) \\ &\times (f(w)-f(q_{0}+k_{0}+w)) \bigg]_{p_{0}=w} \\ &- \epsilon_{3ab} \frac{g_{\rho}^{3}}{2} \int \frac{d^{3}p}{(2\pi)^{3}} \int_{0}^{\infty} \frac{dw}{-\pi} \bigg[ \operatorname{Im}[D_{\pi}(p)] \operatorname{Re}[D_{\pi}(q+p)] \\ &\times \operatorname{Im}[D_{\rho}^{\nu\lambda}(q+k+p)] (-2p-q)_{\mu}(-p+k+q)_{\lambda} \\ &\times (k-q-p)_{\nu} \operatorname{FF}_{\rho}[q+p,k] \operatorname{FF}_{\rho}[p,q+k] \Theta(-q_{0}-k_{0}+w) \\ &\times (f(w)-f(-q_{0}-k_{0}+w)) \bigg]_{p_{0}=-w} , \end{aligned}$$

$$\operatorname{Im}\Gamma^{(3)C\rho k\pi}_{\mu ab3}(k,q) = -\epsilon_{3ab} \frac{g_{\rho}^{3}}{2} \int \frac{d^{3}p}{(2\pi)^{3}} \int_{0}^{\infty} \frac{dw}{-\pi} \bigg[ \operatorname{Im}[D_{\pi}(p)] \operatorname{Im}[D_{\pi}(q-p)] \\ &\times \operatorname{Re}[D_{\rho}^{\nu\lambda}(p+k)] (-2p+q)_{\mu}(-p+k+2q)_{\lambda} \end{aligned}$$

$$\times (k-p)_{v} FF_{\rho}[p,k] FF_{\rho}[-q+p,q+k]$$

$$\times (f(w)-f(q_{0}+w)) \bigg]_{p_{0}=-w},$$

$$(B.5)$$

$$Im\Gamma_{\mu ab3}^{(3)C\rho q\pi}(k,q) = \epsilon_{3ab} \frac{g_{\rho}^{3}}{2} \int \frac{d^{3}p}{(2\pi)^{3}} \int_{0}^{\infty} \frac{dw}{-\pi} \bigg[ Im[D_{\pi}(p)] Im[D_{\pi}(q+p)]$$

$$\times Re[D_{\rho}^{pk}(q+k+p)](-2p-q)_{\mu}(-p+k+q)_{\lambda}(k-q-p)_{v}$$

$$\times FF_{\rho}[q+p,k] FF_{\rho}[p,q+k](f(w)-f(q_{0}+w)) \bigg]_{p_{0}=w},$$

$$(B.6)$$

$$Im\Gamma_{\mu ab3}^{(3)C\sigma k}(k,q) = \epsilon_{3ab} \frac{g_{\rho}g_{\sigma}^{2}}{2} \int \frac{d^{3}p}{(2\pi)^{3}} \int_{0}^{\infty} \frac{dw}{-\pi} \bigg[ Im[D_{\pi}(p)] Re[D_{\pi}(q-p)]$$

$$\times Im[D_{\sigma}(p+k)](p+k)^{2} - m_{\pi}^{2})(-2p+q)_{\mu} FF_{\rho}[p,k]$$

$$\times FF_{\rho}[-q+p,q+k]\Theta(k_{0}+w)(f(w)-f(k_{0}+w)) \bigg]_{p_{0}=w}$$

$$-\epsilon_{3ab} \frac{g_{\rho}g_{\sigma}^{2}}{2} \int \frac{d^{3}p}{(2\pi)^{3}} \int_{0}^{\infty} \frac{dw}{-\pi} \bigg[ Im[D_{\pi}(p)] Re[D_{\pi}(q-p)]$$

$$\times Im[D_{\sigma}(p+k)]((p+k)^{2} - m_{\pi}^{2})(-2p+q)_{\mu} FF_{\rho}[p,k]$$

$$\times FF_{\rho}[-q+p,q+k]\Theta(-k_{0}+w)(f(w)-f(-k_{0}+w)) \bigg]_{p_{0}=-w} .$$

$$(B.7)$$

$$Im\Gamma_{\mu ab3}^{(3)C\sigma q}(k,q) = \epsilon_{3ab} \frac{g_{\rho}g_{\sigma}^{2}}{2} \int \frac{d^{3}p}{(2\pi)^{3}} \int_{0}^{\infty} \frac{dw}{-\pi} \bigg[ Im[D_{\pi}(p)] Re[D_{\pi}(q+p)]$$

$$\times Im[D_{\sigma}(q+k+p)]((q+k+p)^{2} - m_{\pi}^{2})(-2p-q)_{\mu} FF_{\rho}[q+p,k]$$

$$\times FF_{\rho}[p,q+k]\Theta(q_{0}+k_{0}+w)(f(w)-f(q_{0}+k_{0}+w)) \bigg]_{p_{0}=w}$$

$$-\epsilon_{3ab} \frac{g_{\rho}g_{\sigma}^{2}}{2} \int \frac{d^{3}p}{(2\pi)^{3}} \int_{0}^{\infty} \frac{dw}{-\pi} \bigg[ Im[D_{\pi}(p)] Re[D_{\pi}(q+p)]$$

$$\times Im[D_{\sigma}(q+k+p)]((q+k+p)^{2} - m_{\pi}^{2})(-2p-q)_{\mu} FF_{\rho}[q+p,k]$$

$$\times FF_{\rho}[q+k] FF_{\rho}[p,q+k]\Theta(-q_{0}-k_{0}+w)(f(w)$$

$$-f(-q_{0}-k_{0}+w)) \bigg]_{p_{0}=-w} ,$$

$$\times Re[D_{\sigma}(p+k)]((p+k)^{2} - m_{\pi}^{2})(-2p+q)_{\mu} FF_{\sigma}[p,k]$$

$$\times Re[D_{\sigma}(p+k)]((p+k)^{2} - m_{\pi}^{2})(-2p+q)_{\mu} FF_{\sigma}[p,k]$$

$$\times FF_{\sigma}[-q+p,q+k](f(w)-f(q_{0}+w))\Big]_{p_{0}=w},$$
(B.9)  

$$Im\Gamma_{\mu ab3}^{(3)C\sigma q\pi}(k,q) = \epsilon_{3ab} \frac{g_{\rho}g_{\sigma}^{2}}{2} \int \frac{d^{3}p}{(2\pi)^{3}} \int_{0}^{\infty} \frac{dw}{-\pi} \Big[ Im[D_{\pi}(p)]Im[D_{\pi}(q+p)]$$

$$\times Re[D_{\sigma}(q+k+p)]((q+k+p)^{2}-m_{\pi}^{2})(-2p-q)_{\mu}$$

$$\times FF_{\sigma}[q+p,k]FF_{\sigma}[p,q+k](f(w)-f(q_{0}+w)) \Big]_{p_{0}=w}.$$
(B.10)

Here the heaviside step function  $(\Theta)$  is introduced, so that we only include vertex corrections generated by the Landau cut of the pion self-energy.

Next, we address the real parts of the vertex corrections. In the calculation of  $\text{Re}\Sigma_{\pi}$  we never explicitly utilized  $\text{Re}D_{(\rho/\sigma)}$ , opting instead to calculate  $\text{Re}\Sigma_{\pi}$  with subtracted dispersion relations. In order to maintain gauge invariance, we must calculate the vertex corrections with the same  $\text{Re}D_{(\rho/\sigma)}$  as was used in  $\text{Re}\Sigma_{\pi}$ . Thus the real parts of the vertex corrections are also calculated with subtracted dispersion relations:

$$\operatorname{Re}\Gamma_{\mu \, ab3}^{(3)A\rho}(k,q) = \frac{-1}{\pi} \int_{-\infty}^{\infty} dw \left( \frac{\operatorname{Im}\Gamma_{\mu \, ab3}^{(3)A\rho}(\{w,\vec{k}\},q)}{k_0 - w} - \frac{\operatorname{Im}\Gamma_{\mu \, ab3}^{(3)A\rho}(\{w,\vec{k}\},q)}{-w} \right), \tag{B.11}$$

$$\operatorname{Re}\Gamma_{\mu \, ab3}^{(3)B\rho}(k,q) = \frac{-1}{\pi} \int_{-\infty}^{\infty} dw \left( \frac{\operatorname{Im}\Gamma_{\mu \, ab3}^{(3)B\rho}(\{w,\vec{k}\},q)}{k_0 - w} - \frac{\operatorname{Im}\Gamma_{\mu \, ab3}^{(3)B\rho}(\{w,\vec{k}\},q)}{-q_0 - w} \right), \tag{B.12}$$

$$\operatorname{Re}\Gamma^{(3)C(\rho/\sigma)k}_{\mu ab3}(k,q)$$

$$= \frac{-1}{\pi} \int_{-\infty}^{\infty} dw \left( \frac{\mathrm{Im} \Gamma_{\mu \, ab3}^{(3)C(\rho/\sigma)k}(\{w,\vec{k}\},q)}{k_0 - w} - \frac{\mathrm{Im} \Gamma_{\mu \, ab3}^{(3)C(\rho/\sigma)k}\big(\{w,\vec{k}\},q\big)}{-w} \right), \tag{B.13}$$

$${\rm Re}\Gamma^{(3)C(\rho/\sigma)q}_{\mu\,ab3}(k,q)$$

$$= \frac{-1}{\pi} \int_{-\infty}^{\infty} dw \left( \frac{\operatorname{Im}\Gamma_{\mu \, ab3}^{(3)C(\rho/\sigma)q}(\{w,\vec{k}\},q)}{k_0 - w} - \frac{\operatorname{Im}\Gamma_{\mu \, ab3}^{(3)C(\rho/\sigma)q}\left(\{w,\vec{k}\},q\right)}{-q_0 - w} \right), \tag{B.14}$$

$$\operatorname{Re}\Gamma_{\mu \, ab3}^{(3)C(\rho/\sigma)\pi k}(k,q) = \frac{-1}{\pi} \int_{-\infty}^{\infty} dw \frac{\operatorname{Im}\Gamma_{\mu \, ab3}^{(3)C(\rho/\sigma)\pi k}(\{w,\vec{k}\},q)}{k_0 - w}, \tag{B.15}$$

$$\operatorname{Re}\Gamma_{\mu \, ab3}^{(3)C(\rho/\sigma)\pi q}(k,q) = \frac{-1}{\pi} \int_{-\infty}^{\infty} dw \frac{\operatorname{Im}\Gamma_{\mu \, ab3}^{(3)C(\rho/\sigma)\pi q}(\{w,\vec{k}\},q)}{k_0 - w} \,. \tag{B.16}$$

The subtractions are determined by the argument of the  $\rho$  or  $\sigma$  propagator in the vertex correction, and are fixed by the subtractions used in the pion self-energy. Notably,  $\text{Re}\Gamma^{(3)C(\rho/\sigma)\pi(k/q)}_{\mu\,ab3}$  does not include a subtraction, because it is not proportional to  $\text{Re}D_{(\rho/\sigma)}$ . Instead,  $\text{Re}\Gamma^{(3)C(\rho/\sigma)\pi(k/q)}_{\mu\,ab3}$  is proportional to  $\text{Im}D_{(\rho/\sigma)}$  and  $\text{Im}\Gamma^{(3)C(\rho/\sigma)\pi(k/q)}_{\mu\,ab3}$  is proportional to  $\text{Re}D_{(\rho/\sigma)}$ . Thus, to maintain consistent  $\rho$  and  $\sigma$  propagators we perform a subtraction on  $\text{Im}\Gamma^{(3)C(\rho/\sigma)\pi(k/q)}_{\mu\,ab3}$ , rather than  $\text{Re}\Gamma^{(3)C(\rho/\sigma)\pi(k/q)}_{\mu\,ab3}$ .

$$\operatorname{Im}\tilde{\Gamma}_{\mu\,ab3}^{(3)C\rho\pi k}(k,q) = \operatorname{Im}\Gamma_{\mu\,ab3}^{(3)C(\rho/\sigma)\pi k}(k,q) - \operatorname{Im}\Gamma_{\mu\,ab3}^{(3)C\rho\pi k}(\{k_0=0,\vec{k}\},q), \tag{B.17}$$

$$\operatorname{Im}\tilde{\Gamma}_{\mu \, ab3}^{(3)C\rho\pi q}(k,q) = \operatorname{Im}\Gamma_{\mu \, ab3}^{(3)C(\rho/\sigma)\pi q}(k,q) - \operatorname{Im}\Gamma_{\mu \, ab3}^{(3)C\rho\pi q}(\{k_0 = -q_0, \vec{k}\}, q), \tag{B.18}$$

$$\operatorname{Im} \tilde{\Gamma}_{\mu \, ab3}^{(3)C\sigma\pi k}(k,q) = \operatorname{Im} \Gamma_{\mu \, ab3}^{(3)C(\rho/\sigma)\pi k}(k,q) - \operatorname{Im} \Gamma_{\mu \, ab3}^{(3)C\sigma\pi k}(\{k_0 = 0, \vec{k}\}, q),$$

$$\operatorname{Im} \tilde{\Gamma}_{\mu \, ab3}^{(3)C\sigma\pi q}(k,q) = \operatorname{Im} \Gamma_{\mu \, ab3}^{(3)C(\rho/\sigma)\pi q}(k,q) - \operatorname{Im} \Gamma_{\mu \, ab3}^{(3)C\sigma\pi q}(\{k_0 = -q_0, \vec{k}\}, q).$$
(B.20)

$$\operatorname{Im} \tilde{\Gamma}_{\mu \, ab3}^{(3)C\sigma\pi q}(k,q) = \operatorname{Im} \Gamma_{\mu \, ab3}^{(3)C(\rho/\sigma)\pi q}(k,q) - \operatorname{Im} \Gamma_{\mu \, ab3}^{(3)C\sigma\pi q}(\{k_0 = -q_0, \vec{k}\}, q). \tag{B.20}$$

The subtractions allow for a straightforward implementation of spectral representations, without introducing an additional violation of gauge invariance. The spectral representations are given by:

$$D_{\pi}(k)\Gamma_{\mu\,ab3}^{(3)k}(k,q) = \frac{-1}{\pi} \int_{-\pi}^{\infty} dv \frac{\text{Im}\left[D_{\pi}(v,\vec{k})\Gamma_{\mu\,ab3}^{(3)k}(\{v,\vec{k}\},q)\right]}{k_0 - v + i\epsilon},$$
(B.21)

$$D_{\pi}(q+k)\Gamma_{\mu\,ab3}^{(3)q}(q+k,q) = \frac{-1}{\pi} \int_{-\infty}^{\infty} dv' \frac{\text{Im}\left[D_{\pi}(v',\vec{k})\Gamma_{\mu\,ab3}^{(3)q}(\{v',\vec{k}\},q)\right]}{q_0 + k_0 - v' + i\epsilon},\tag{B.22}$$

$$D_{\pi}(k)\Gamma_{\mu ab3}^{(3)k}(k,q)^{2} = \frac{-1}{\pi} \int_{-\infty}^{\infty} dv \frac{\text{Im}\left[D_{\pi}(v,\vec{k})\Gamma_{\mu ab3}^{(3)k}(\{v,\vec{k}\},q)^{2}\right]}{k_{0} - v + i\epsilon},$$
 (B.23)

$$D_{\pi}(q+k)\Gamma_{\mu\,ab3}^{(3)q}(q+k,q)^{2} = \frac{-1}{\pi} \int_{-\infty}^{\infty} dv' \frac{\text{Im}\left[D_{\pi}(v',\vec{k})\Gamma_{\mu\,ab3}^{(3)q}(\{v',\vec{k}\},q)^{2}\right]}{q_{0}+k_{0}-v'+i\epsilon} , \qquad (B.24)$$

where we define the functions:

$$\begin{split} \Gamma^{(3)k}_{\mu\,ab3}(k,q) &= \Gamma^{(3)A\rho}_{\mu\,ab3}(k,q) + \Gamma^{(3)C\rho k}_{\mu\,ab3}(k,q) + \tilde{\Gamma}^{(3)C\rho k\pi}_{\mu\,ab3}(k,q) + \Gamma^{(3)C\sigma k\pi}_{\mu\,ab3}(k,q) \\ &+ \tilde{\Gamma}^{(3)C\sigma k\pi}_{\mu\,ab3}(k,q) + g_{\rho}\epsilon_{3ab}(2k+q)_{i} \bigg( \frac{\Sigma_{\pi(\rho)}(k)}{\Lambda_{2\rho}^{2} + (\vec{q} + \vec{k})^{2}} + \frac{\Sigma_{\pi(\sigma)}(k)}{\Lambda_{2\sigma}^{2} + (\vec{q} + \vec{k})^{2}} \bigg), \end{split} \tag{B.25}$$

$$\begin{split} \Gamma^{(3)q}_{\mu\,ab3}(k,q) &= \Gamma^{(3)B\rho}_{\mu\,ab3}(-q+k,q) + \Gamma^{(3)C\rho q}_{\mu\,ab3}(-q+k,q) + \tilde{\Gamma}^{(3)C\rho q\pi}_{\mu\,ab3}(-q+k,q) \\ &+ \Gamma^{(3)C\sigma q}_{\mu\,ab3}(-q+k,q) + \tilde{\Gamma}^{(3)C\sigma q\pi}_{\mu\,ab3}(-q+k,q) \\ &+ g_{\rho}\epsilon_{3ab}(2k-q)_{i} \left(\frac{\Sigma_{\pi(\rho)}(k)}{\Lambda_{2\rho}^{2} + (\vec{k})^{2}} + \frac{\Sigma_{\pi(\sigma)}(k)}{\Lambda_{2\sigma}^{2} + (\vec{k})^{2}}\right). \end{split} \tag{B.26}$$

The real part of the integrals in eqs. (B.21) through (B.24) are calculated from the principal values of the integrals.

We are now in place to calculate the transverse projection of the  $\pi\pi$ -loop diagrams containing vertex corrections, at  $\vec{q} = 0$ . In terms of  $\Gamma^{(3)k}_{\mu ab3}$  and  $\Gamma^{(3)q}_{\mu ab3}$  one can write the transverse projection of the vertex corrections to the  $\pi\pi$ -loop as

$$\Sigma_{\rho 1}(q_0, \vec{q} = 0) = \frac{2\pi}{3} T \sum_{n(even)} \int \frac{d|\vec{k}|\vec{k}^2}{(2\pi)^3} \int_{-\infty}^{\infty} \frac{dv dv'}{\pi^2} \frac{1}{(k_0 - v + i\epsilon)(q_0 + k_0 - v' + i\epsilon)} \left[ 2g_{\rho} \epsilon_{3ab}(2|\vec{k}|) \text{Im}[D_{\pi}(v, \vec{k}) \Gamma_{3ba3}^{(3)k}(\{v, \vec{k}\}, q)] \text{Im}[D_{\pi}(v', \vec{k})] \right]$$

$$+2g_{\rho}\epsilon_{3ab}(2|\vec{k}|)\mathrm{Im}[D_{\pi}(v,\vec{k})]\mathrm{Im}[D_{\pi}(v',\vec{k})\Gamma_{3ba3}^{(3)q}(\{v',\vec{k}\},q)]$$

$$+2\mathrm{Im}[D_{\pi}(v,\vec{k})\Gamma_{3ab3}^{(3)k}(\{v,\vec{k}\},q)]\mathrm{Im}[D_{\pi}(v',\vec{k})\Gamma_{3ba3}^{(3)q}(\{v',\vec{k}\},q)]$$

$$-\mathrm{Im}[D_{\pi}(v,\vec{k})(\Gamma_{3ab3}^{(3)k}(\{v,\vec{k}\},q))^{2}]\mathrm{Im}[D_{\pi}(v',\vec{k})]$$

$$-\mathrm{Im}[D_{\pi}(v,\vec{k})]\mathrm{Im}[D_{\pi}(v',\vec{k})(\Gamma_{3ab3}^{(3)q}(\{v',\vec{k}\},q))^{2}]\Big]_{ko=io_{\pi}} + \mathrm{PV} \cdot (\mathrm{B.27})$$

One can now perform the Matsubara sum to obtain

$$\begin{split} \Sigma_{\rho 1}(q_{0},\vec{q}=0) &= \frac{-2\pi}{3} \int \frac{d|\vec{k}|\vec{k}^{2}}{(2\pi)^{3}} \int_{-\infty}^{\infty} \frac{dvdv'}{\pi^{2}} \frac{(f(v)-f(v'))}{q_{0}+v-v'} \\ & \left[ 2g_{\rho}\epsilon_{3ab}(2|\vec{k}|) \text{Im}[D_{\pi}(v,\vec{k})\Gamma_{3ba3}^{(3)k}(\{v,\vec{k}\},q)] \text{Im}[D_{\pi}(v',\vec{k})] \\ & + 2g_{\rho}\epsilon_{3ab}(2|\vec{k}|) \text{Im}[D_{\pi}(v,\vec{k})] \text{Im}[D_{\pi}(v',\vec{k})\Gamma_{3ba3}^{(3)q}(\{v',\vec{k}\},q)] \\ & + 2\text{Im}[D_{\pi}(v,\vec{k})\Gamma_{3ab3}^{(3)k}(\{v,\vec{k}\},q)] \text{Im}[D_{\pi}(v',\vec{k})\Gamma_{3ba3}^{(3)q}(\{v',\vec{k}\},q)] \\ & - \text{Im}[D_{\pi}(v,\vec{k})(\Gamma_{3ab3}^{(3)k}(\{v,\vec{k}\},q))^{2}] \text{Im}[D_{\pi}(v',\vec{k}),q)^{2}] \Big] + \text{PV} \,, \end{split} \tag{B.28}$$

where PV denotes the Paulli-Villars regularization terms, defined by dressing the vacuum Pauli-Villars terms with thermal-pion self-energies and vertex corrections. Finally, we remove doublecounting introduced by  $\Gamma^{(3)C(\rho/\sigma)}_{\mu ab3}$  from the Landau cut of  $\Sigma_{\rho 1}$ . This is achieved by introducing a function,  $\tilde{\Sigma}_{\rho 1}$ , which subtracts the double-counting,

$$\tilde{\Sigma}_{\rho 1}(q_{0}, \vec{q} = 0) = \frac{2\pi}{3} \int \frac{d|\vec{k}|\vec{k}^{2}}{(2\pi)^{3}} \int_{-\infty}^{\infty} \frac{dv dv'}{\pi^{2}} \frac{\Theta(vv')(f(v) - f(v'))}{q_{0} + v - v'} \\
\left[ g_{\rho} \epsilon_{3ab}(2|\vec{k}|) \text{Im}[D_{\pi}(v, \vec{k}) \chi^{k}(\{v, \vec{k}\}, q)] \text{Im}[D_{\pi}(v', \vec{k})] \\
+ g_{\rho} \epsilon_{3ab}(2|\vec{k}|) \text{Im}[D_{\pi}(v, \vec{k})] \text{Im}[D_{\pi}(v', \vec{k}) \chi^{q}(\{v', \vec{k}\}, q)] \right], \tag{B.29}$$

where

$$\chi^{k}(k,q) = \Gamma_{3ba3}^{(3)C\rho k}(k,q) + \tilde{\Gamma}_{3ba3}^{(3)C\rho k\pi}(k,q),$$

$$\chi^{q}(k,q) = \Gamma_{3ba3}^{(3)C\rho q}(-q+k,q) + \tilde{\Gamma}_{3ba3}^{(3)C\rho q\pi}(-q+k,q).$$
(B.30)
(B.31)

$$\chi^{q}(k,q) = \Gamma_{3hq3}^{(3)C\rho q}(-q+k,q) + \tilde{\Gamma}_{3hq3}^{(3)C\rho q\pi}(-q+k,q). \tag{B.31}$$

### B.2. Tadpole loop corrections

In this section we give the corrections to the tadpole loop from the  $\rho\rho\pi\pi$  vertex corrections. To begin, we consider  $\Gamma^{(4)A\rho}_{\mu\nu\,ab33}$ , which we rewrite in terms of a function  $\tilde{\Gamma}^{(4)A\rho}_{\mu\nu\,ab33}$  such that

$$\Gamma^{(4)A\rho}_{\mu\nu\,ab33}(k,q) = i \left( \tilde{\Gamma}^{(4)A\rho}_{\mu\nu\,ab33}(k,q) + \tilde{\Gamma}^{(4)A\rho}_{\mu\nu\,ab33}(-k,q) \right). \tag{B.32}$$

We have factored a complex i out of the vertex correction, so that it more closely resembles the vacuum  $\pi\pi\rho\rho$  vertex. Additionally, it is more convenient to define spectral representations in terms of  $\tilde{\Gamma}^{(4)A\rho}_{\mu\nu\,ab33}$ . The imaginary part of  $\tilde{\Gamma}^{(4)A\rho}_{\mu\nu\,ab33}$  is given by

$$\begin{split} \operatorname{Im} \tilde{\Gamma}^{(4)A\rho}_{\mu\nu\,ab33}(k,q) &= (3\delta_{3a}\delta_{3b} - 5\delta_{ab}) \frac{g_{\rho}^{4}}{2} \int \frac{d^{3}p}{(2\pi)^{3}} \bigg[ \int_{0}^{\infty} \frac{dw}{-\pi} \operatorname{Im}[D_{\pi}(p)] \operatorname{Im}[D_{\rho}^{\mu\nu}(q+k+p)] \\ &\times (f(w) - f(q_{0} + k_{0} + w)) \Theta(q_{0} + k_{0} + w) \operatorname{FF}_{\rho}[q+p,k]^{2} \bigg]_{p_{0} = w} \\ &- (3\delta_{3a}\delta_{3b} - 5\delta_{ab}) \frac{g_{\rho}^{4}}{2} \int \frac{d^{3}p}{(2\pi)^{3}} \bigg[ \int_{0}^{\infty} \frac{dw}{-\pi} \operatorname{Im}[D_{\pi}(p)] \operatorname{Im}[D_{\rho}^{\mu\nu}(q+k+p)] \\ &\times (f(w) - f(-q_{0} - k_{0} + w)) \Theta(-q_{0} - k_{0} + w) \operatorname{FF}_{\rho}[q+p,k]^{2} \bigg]_{p_{0} = -w} , \end{split}$$

$$(B.33)$$

where we only write the cuts necessary to maintain gauge invariance. The real part of  $\Gamma^{(4)A\rho}_{\mu\nu\,ab33}$  can be calculated with a subtracted dispersion relation,

$$\operatorname{Re}\tilde{\Gamma}^{(4)A\rho}_{\mu\nu\,ab33} = \frac{-1}{\pi} \int_{-\infty}^{\infty} dw \left( \frac{\operatorname{Im}\tilde{\Gamma}^{(4)A\rho}_{\mu\nu\,ab33}(\{w,\vec{k}\},q)}{k_0 - w} - \frac{\operatorname{Im}\tilde{\Gamma}^{(4)A\rho}_{\mu\nu\,ab33}(\{w,\vec{k}\},q)}{-q_0 - w} \right). \tag{B.34}$$

The transverse projection of the  $\rho$  self-energy corrections derived from  $\Gamma^{(4)A\rho}_{\mu\nu\,ab33}$  at  $\vec{q}=0$  are given by

$$\begin{split} \Sigma_{\rho 2}(q_{0},0) &= \frac{4\pi}{3} T \sum_{n(even)} \int \frac{d|\vec{k}|\vec{k}^{2}}{(2\pi)^{3}} \int_{-\infty}^{\infty} \frac{dv dv'}{\pi^{2}} \text{Im}[D_{\pi}(v,\vec{k})] \text{Im}[\tilde{\Gamma}_{ii\,aa33}^{(4)A\rho}(\{-q_{0}+v',\vec{k}\},q)] \\ &\times \frac{1}{(i\omega_{n}-v+i\epsilon)(q_{0}+i\omega_{n}-v'+i\epsilon)} + \text{PV} \\ &= \frac{-4\pi}{3} \int \frac{d|\vec{k}|\vec{k}^{2}}{(2\pi)^{3}} \int_{-\infty}^{\infty} \frac{dv dv'}{\pi^{2}} \text{Im}[D_{\pi}(v,\vec{k})] \text{Im}[\tilde{\Gamma}_{ii\,aa33}^{(4)A\rho}(\{-q_{0}+v',\vec{k}\},q)] \\ &\times \frac{1}{q_{0}+v-v'+i\epsilon} (1-\frac{1}{2}\Theta(vv'))(f(v)-f(v')) + \text{PV}, \end{split} \tag{B.35}$$

$$\Sigma_{\rho 2}^{0} &= \frac{4\pi}{3} T \sum_{n(even)} \int \frac{d|\vec{k}|\vec{k}^{2}}{(2\pi)^{3}} \int_{-\infty}^{\infty} \frac{dv}{-\pi} \text{Re}[\tilde{\Gamma}_{ii\,aa33}^{(4)A\rho}(\{0,\vec{k}\},0)] \frac{\text{Im}[D_{\pi}(v,\vec{k})]}{(i\omega_{n}-v+i\epsilon)} + \text{PV} \\ &= -\frac{4\pi}{3} \int \frac{d|\vec{k}|\vec{k}^{2}}{(2\pi)^{3}} \int_{-\infty}^{\infty} \frac{dv}{-\pi} \text{Re}[\tilde{\Gamma}_{ii\,aa33}^{(4)A\rho}(\{0,\vec{k}\},0)] \\ &\times \text{Im}[D_{\pi}(v,\vec{k})](1-\frac{1}{2}\Theta(v))f(v) + \text{PV}, \end{split} \tag{B.36}$$

where the theta functions are added in the last equalities to remove double-counting from the Landau cut, as was described in appendix A.3. Unlike the corrections to the  $\rho\pi\pi$  vertex,  $\tilde{\Gamma}^{(4)A\rho}_{ii\,aa33}$  introduces a nondispersive constant into the rho self-energy. Thus we explicitly calculated this constant with  $\Sigma^0_{\rho 2}$ .

The corrections to the tadpole diagram due to the addition of a form factor can be expressed in a similar form. We write these contributions in terms of the following functions

$$\begin{split} Y_k(k,\{q_0,\vec{q}=0\}) &= -\frac{4g_\rho\epsilon_{3ca}k_3}{\Lambda_{2\rho}^2 + \vec{k}^2} \bigg[ \Gamma_{3ac3}^{(3)A\rho}(k,q) + \Gamma_{3ac3}^{(3)C\rho k}(k,q) + \Gamma_{3ac3}^{\prime\prime(3)C\rho k\pi}(k,q) \bigg] \\ &- \frac{4g_\rho\epsilon_{3ca}k_3}{\Lambda_{2\sigma}^2 + \vec{k}^2} \bigg[ \Gamma_{3ac3}^{(3)C\sigma k}(k,q) + \Gamma_{\mu ac3}^{(3)C\sigma k\pi}(k,q) \bigg] \\ &- 4g_\rho^2 \bigg\{ 4k_3^2 \bigg[ \frac{\Sigma_{\pi(\rho)}(k)}{(\Lambda_{2\rho}^2 + \vec{k}^2)^2} + \frac{\Sigma_{\pi(\sigma)}(k)}{(\Lambda_{2\sigma}^2 + \vec{k}^2)^2} \bigg] \\ &- 3\frac{\Sigma_{\pi(\rho)}(k)}{\Lambda_{2\rho}^2 + \vec{k}^2} - 3\frac{\Sigma_{\pi(\sigma)}(k)}{\Lambda_{2\sigma}^2 + \vec{k}^2} \bigg\}, \end{split} \tag{B.37}$$
 
$$Y_q(k,\{q_0,\vec{q}=0\}) = -\frac{4g_\rho\epsilon_{3ca}k_3}{\Lambda_{2\rho}^2 + \vec{k}^2} \bigg[ \Gamma_{3ab3}^{(3)B\rho}(-q+k,q) + \Gamma_{3ab3}^{(3)C\rho q}(-q+k,q) \\ &+ \Gamma_{3ab3}^{(3)C\rho q\pi}(-q+k,q) \bigg] - \frac{4g_\rho\epsilon_{3ca}k_3}{\Lambda_{2\sigma}^2 + \vec{k}^2} \bigg[ \Gamma_{3ab3}^{(3)C\sigma q}(-q+k,q) \\ &+ \Gamma_{3ab3}^{(3)C\sigma q\pi}(-q+k,q) \bigg] \\ &- 8g_\rho^2k_3^2 \bigg[ \frac{\Sigma_{\pi(\rho)}(k)}{(\Lambda_{2\rho}^2 + \vec{k}^2)^2} + \frac{\Sigma_{\pi(\sigma)}(k)}{(\Lambda_{2\sigma}^2 + \vec{k}^2)^2} \bigg] \,. \tag{B.38} \end{split}$$

The transverse projection of the corresponding  $\rho$  self-energy contributions at  $\vec{q} = 0$  is given by

$$\begin{split} \Sigma_{\rho 3}(q_{0},0) &= \frac{2\pi}{3} T \sum_{n(even)} \int \frac{d|\vec{k}|\vec{k}^{2}}{(2\pi)^{3}} \Big[ D_{\pi}(k) \big( Y_{q}(q+k,q) + Y_{q}(q-k,q) \\ &+ Y_{k}(k,q) + Y_{k}(-k,q) \big) \Big]_{k_{0} = i\omega_{n}} \\ &= \frac{-4\pi}{3} \int \frac{d|\vec{k}|\vec{k}^{2}}{(2\pi)^{3}} \int_{-\infty}^{\infty} \frac{dv dv'}{\pi^{2}} \mathrm{Im}[Y_{q}(\{v',\vec{k}\},q)] \mathrm{Im}[D_{\pi}(v,\vec{k})] \\ &\times \frac{1}{q_{0} + v - v' + i\epsilon} (f(v) - f(v')) + \mathrm{PV}, \\ \Sigma_{\rho 3}^{0} &= \frac{4\pi}{3} T \sum_{n(even)} \int \frac{d|\vec{k}|\vec{k}^{2}}{(2\pi)^{3}} \int_{-\infty}^{\infty} \frac{dv}{-\pi} \mathrm{Re}[Y_{q}(\{0,\vec{k}\},0)] \frac{\mathrm{Im}[D_{\pi}(v,\vec{k})]}{(i\omega_{n} - v + i\epsilon)} \\ &+ \frac{4\pi}{3} T \sum_{n(even)} \int \frac{d|\vec{k}|\vec{k}^{2}}{(2\pi)^{3}} \int_{-\infty}^{\infty} \frac{dv}{-\pi} \frac{\mathrm{Im}[Y_{k}(\{v,\vec{k}\},0)D_{\pi}(v,\vec{k})]}{(i\omega_{n} - v + i\epsilon)} \\ &= -\frac{4\pi}{3} \int \frac{d|\vec{k}|\vec{k}^{2}}{(2\pi)^{3}} \int_{-\infty}^{\infty} \frac{dv}{-\pi} \mathrm{Re}[Y_{q}(\{0,\vec{k}\},0)] \mathrm{Im}[D_{\pi}(v,\vec{k})] f(v) \end{split}$$

$$-\frac{4\pi}{3} \int \frac{d|\vec{k}|\vec{k}^2}{(2\pi)^3} \int_{-\infty}^{\infty} \frac{dv}{-\pi} \text{Im} \left[ Y_k(\{v, \vec{k}\}, 0) D_{\pi}(v, \vec{k}) \right] f(v) + \text{PV} , \qquad (B.40)$$

where we again explicitly calculate a nondispersive constant with  $\Sigma_{\rho 3}^{0}$ .

Next, we calculate corrections to the tadpole that can be expressed in terms of unitarity cuts of  $\rho\pi$  or  $\sigma\pi$ -loops,  $\Gamma^{(4)B_1\rho}_{\mu\nu\,ab33}$ ,  $\Gamma^{(4)B_2\rho}_{\mu\nu\,ab33}$ ,  $\Gamma^{(4)E\rho}_{\mu\nu\,ab33}$ ,  $\Gamma^{(4)E\rho}_{\mu\nu\,ab33}$ ,  $\Gamma^{(4)E\sigma}_{\mu\nu\,ab33}$ , and  $\Gamma^{(4)G\sigma}_{\mu\nu\,ab33}$ . These  $\rho$  self-energies dress a pion propagator with the unitarity cut of the pion self-energy  $(\Sigma^U_{\pi})$ . For positive energy  $\mathrm{Im}\Sigma^U_{\pi}(R)$  is given by

$$\operatorname{Im}\Sigma_{\pi\rho}^{U(R)}(k,T) = g_R^2 \int \frac{d^3p}{(2\pi)^3} \int_0^\infty \frac{dw}{-\pi} \Big[ -\Theta(k_0 - w) \operatorname{Im}[D_{\pi}(p)] \operatorname{Im}[D_R(k+p)] \\ \times N_{R\pi\pi}[p,k,p_0 + k_0] \operatorname{FF}_R[p,k]^2 (1 + f(w) + f(k_0 - w)) \Big]_{p_0 = -w},$$
(B.41)

For negative energies,  $\Sigma_{\pi}^{U}$  is determined by forcing the imaginary part of the pion self-energy to be odd, that is enforcing the retarded property of the pion self-energy. The real part of  $\Sigma_{\pi}^{U}$  can then be evaluated with the dispersion relation

$$\operatorname{Re}\Sigma_{\pi}^{U}(k) = \frac{-1}{\pi} \operatorname{p.v.} \int_{0}^{\infty} dv^{2} \frac{\operatorname{Im}\Sigma_{\pi}^{U}(v,\vec{k})}{k_{0}^{2} - v^{2}} - \frac{\operatorname{Im}\Sigma_{\pi}^{U}(v,\vec{k})}{-v^{2}} . \tag{B.42}$$

However, this dispersion relation converges quite slowly, resulting in an unphysical shift of the pion mass by approximately 800 MeV. The shift is produced by vacuum  $\pi \to \rho \pi$  and  $\pi \to \sigma \pi$  decays and in principal should be absorbed into the pion mass; however, modifying the real part of the vacuum loop in only these diagrams would violate gauge invariance. In order to remove the shift systematically, while preserving gauge invariance, we resum the pion propagators in the  $\rho$  self-energy with  $\Sigma_\pi^U$  yielding

$$\begin{split} & \Sigma_{\rho\,U}^{\mu\nu}(q) \\ &= g_{\rho}^2 \int \frac{d^3k}{(2\pi)^3} \int\limits_{-\infty}^{\infty} \frac{dv dv'}{\pi^2} \frac{(2k+q)^{\mu}(2k+q)^{\nu}}{q_0 + v - v' + i\epsilon} (f(v) - f(v'))\Theta(vv') \\ & \times \mathrm{Im} [\frac{1}{v^2 - \vec{k}^2 - m_{\pi}^2 - \Sigma_{\pi}(v, \vec{k}, T) - \Sigma_{\pi}^U(v, \vec{k}, T) - \mathrm{Re}\Sigma_{\pi}^U(m_{\pi}, 0, 0)}] \\ & \times \mathrm{Im} [\frac{1}{(v')^2 - (\vec{q} + \vec{k})^2 - m_{\pi}^2 - \Sigma_{\pi}(v', \vec{q} + \vec{k}, T) - \Sigma_{\pi}^U(v', \vec{q} + \vec{k}, T) - \mathrm{Re}\Sigma_{\pi}^U(m_{\pi}, 0, 0)}] \\ & - 2g_{\rho}^2 g^{\mu\nu} \int \frac{d^3k}{(2\pi)^3} \int\limits_{-\infty}^{\infty} \frac{dv}{-\pi} f(v)\Theta(v) \\ & \times \mathrm{Im} [\frac{1}{v^2 - \vec{k}^2 - m_{\pi}^2 - \Sigma_{\pi}(v, \vec{k}, T) - \Sigma_{\pi}^U(v, \vec{k}, T) - \mathrm{Re}\Sigma_{\pi}^U(m_{\pi}, 0, 0)}], \end{split} \tag{B.43}$$

where we have limited the integration with theta functions to ensure that we do not introduce new vacuum  $\rho$  self-energy diagrams. Finally, we apply Pauli-Villars regularization to the vacuum  $\Sigma_{\pi}^{U}$  loop, such that

$$\operatorname{Im}\Sigma_{\pi}^{U}(k, m_{\pi}, T) \to \operatorname{Im}\Sigma_{\pi}^{U}(k, m_{\pi}, T) - 2\operatorname{Im}\Sigma_{\pi}^{U}(k, \sqrt{m_{\pi}^{2} + \Lambda_{0}^{2}}, T = 0)$$
 (B.44)

$$+\mathrm{Im}\Sigma_{\pi}^{U}(k,\sqrt{m_{\pi}^{2}+2\Lambda_{0}^{2}},T=0)$$
 (B.45)

Equation (B.43) contains the tadpole corrections derived from  $\Gamma^{(4)E\rho}_{\mu\nu ab33}$ ,  $\Gamma^{(4)G\rho}_{\mu\nu ab33}$ ,  $\Gamma^{(4)E\sigma}_{\mu\nu ab33}$ , and  $\Gamma^{(4)G\sigma}_{\mu\nu ab33}$  in the resummation of the pion propagator. However, in Eq. (B.43) we are free to treat  $\Sigma^U_{\pi}$  equivalently to  $\Sigma_{\pi}$ , performing a zero-energy subtraction on  $\text{Re}\Sigma^U_{\pi}$ . Furthermore, we add a constant shift  $\text{Re}\Sigma^U_{\pi}(k_0=m_{\pi},\vec{k}=0,T=0)$  to ensure that the vacuum pion mass is 140 MeV at  $\vec{p}=0$ . We are able add this constant without violating gauge invariance, because it simply amounts to a redefinition of the bare pion mass. It should be noted that because we have dressed the pion propagators with  $\Sigma^U_{\pi}$  the Ward identities imply that additional vertex corrections must be calculated to maintain gauge invariance. These additional corrections correspond to the unitarity cuts of the previously calculated thermal vertex corrections. However, we have already encountered these corrections by dressing the unitarity cut of the  $\rho$  self-energy with thermal vertex corrections. This symmetry is precisely why double-counting was encountered in the Landau cut. In fact, the first-order corrections to the resummation in Eq. (B.43) are already included in our formalism, and attempting to explicitly calculate first-order vertex corrections due to  $\Sigma^U_{\pi}$  would only introduce double-counting into the unitarity cut of  $\Sigma^{\mu\nu}_{\rho}$ .

We now take the transverse projections of  $\Sigma_{oU}^{\mu\nu}$ , at  $\vec{q}=0$  to obtain

$$\begin{split} & \Sigma_{\rho 4}(q_{0},0) \\ & = \frac{4\pi g_{\rho}^{2}}{3} \int \frac{dk\vec{k}^{2}}{(2\pi)^{3}} \int_{-\infty}^{\infty} \frac{dvdv'}{\pi^{2}} \frac{4\vec{k}^{2}\Theta(vv')(f(v)-f(v'))}{q_{0}+v-v'+i\epsilon} \\ & \times \mathrm{Im} [\frac{1}{v^{2}-\vec{k}^{2}-m_{\pi}^{2}-\Sigma_{\pi}(v,\vec{k},T)-\Sigma_{\pi}^{U}(v,\vec{k},T)-\mathrm{Re}\Sigma_{\pi}^{U}(m_{\pi},0,0)}] \\ & \times \mathrm{Im} [\frac{1}{(v')^{2}-(\vec{q}+\vec{k})^{2}-m_{\pi}^{2}-\Sigma_{\pi}(v',\vec{q}+\vec{k},T)-\Sigma_{\pi}^{U}(v',\vec{q}+\vec{k},T)-\mathrm{Re}\Sigma_{\pi}^{U}(m_{\pi},0,0)}] \\ & \Sigma_{\rho 4}^{0}(q_{0},0) = -\frac{8g_{\rho}^{2}}{3} \int \frac{dk\vec{k}^{2}}{(2\pi)^{3}} \\ & \times \int_{-\infty}^{\infty} \frac{dv}{-\pi} \mathrm{Im} [\frac{f(v)\Theta(v)}{v^{2}-\vec{k}^{2}-m_{\pi}^{2}-\Sigma_{\pi}(v,\vec{k},T)-\Sigma_{\pi}^{U}(v\vec{k},T)-\mathrm{Re}\Sigma_{\pi}^{U}(m_{\pi},0,0)}], \end{split} \tag{B.47}$$

where  $\Sigma_{o4}^{0}$  again calculates a nondispersive constant.

Finally, we calculate the  $\rho$  self-energy corrections due to  $\Gamma^{(4)B_1\rho}_{\mu\nu\,ab33}$  and  $\Gamma^{(4)B_2\rho}_{\mu\nu\,ab33}$ . These corrections can be expressed in terms of the unitarity cut of  $\Gamma^{(3)A\rho}_{\mu\,ab3}$  as

$$\begin{split} & \operatorname{Im} \Gamma^{(3)AU\rho}_{\mu \, ab3}(k,q) \\ &= \epsilon_{3ab} \frac{3g_{\rho}^{3}}{2} \int \frac{d^{3}p}{(2\pi)^{3}} \int_{0}^{\infty} \frac{dw}{-\pi} \bigg[ \operatorname{Im}[D_{\pi}(p)] \operatorname{Im}[D_{\rho}^{\nu\lambda}(p+k)] g_{\mu\lambda}(k-p)_{\nu} \\ & \times \operatorname{FF}_{\rho}[-q+p,q+k] \operatorname{FF}_{\rho}[p,k] \Theta(k_{0}-w) (1+f(w)+f(k_{0}-w)) \bigg]_{p_{0}=-w} \\ & -\epsilon_{3ab} \frac{3g_{\rho}^{3}}{2} \int \frac{d^{3}p}{(2\pi)^{3}} \int_{0}^{\infty} \frac{dw}{-\pi} \bigg[ \operatorname{Im}[D_{\pi}(p)] \operatorname{Im}[D_{\rho}^{\nu\lambda}(p+k)] g_{\mu\lambda}(k-p)_{\nu} \\ & \times \operatorname{FF}_{\rho}[-q+p,q+k] \operatorname{FF}_{\rho}[p,k] \Theta(-k_{0}-w) (1+f(w)+f(-k_{0}-w)) \bigg]_{p_{0}=w} \\ & -2 \bigg[ m_{\pi} \to \sqrt{m_{\pi}^{2} + \Lambda_{0}^{2}} \bigg]_{T=0} + \bigg[ m_{\pi} \to \sqrt{m_{\pi}^{2} + 2\Lambda_{0}^{2}} \bigg]_{T=0} \,, \end{split} \tag{B.48}$$

where the last line implements the Pauli-Villars regularization on the vacuum loop. The real part of  $\Gamma_{\mu,ab3}^{(3)AU\rho}$  is given by the subtracted dispersion relation

$$\operatorname{Re}\Gamma_{\mu \, ab3}^{(3)AU\rho}(k,q) = \frac{-1}{\pi} \text{p.v.} \int_{-\infty}^{\infty} dv \frac{\operatorname{Im}\Gamma_{\mu \, ab3}^{(3)AU\rho}(\{v,\vec{k}\},q)}{k_0 - v} - \frac{\operatorname{Im}\Gamma_{\mu \, ab3}^{(3)AU\rho}(\{v,\vec{k}\},q)}{-v} \ . \tag{B.49}$$

The self-energy correction arising from  $\Gamma^{(4)B_1\rho}_{\mu\nu\,ab33}$  and  $\Gamma^{(4)B_2\rho}_{\mu\nu\,ab33}$  is then given by

$$\Sigma_{\rho 5}(q_{0},0) = \frac{-8\pi}{3} \int \frac{d|\vec{k}|\vec{k}^{2}}{(2\pi)^{3}} \int_{-\infty}^{\infty} \frac{dv dv'}{\pi^{2}} \text{Im}[D_{\pi}(v',\vec{k})] \text{Im}[D_{\pi}(v,\vec{k})\Gamma_{3ba}^{(3)AU\rho}(v,\vec{k})]$$

$$\times (2g_{\rho}|\vec{k}|\epsilon_{3ab}) \frac{(f(v) - f(v'))}{(q_{0} + v - v' + i\epsilon)} \Theta(vv') , \qquad (B.50)$$

where we again limit our calculation to the Landau cut of  $\Sigma_{\rho}^{\mu\nu}$ .

### B.3. Total corrections

The total contribution of the vertex corrections to the transverse projections of the  $\rho$  self-energy, at  $\vec{q} = 0$ , is given by

$$\Sigma_{\rho}^{VC}(q_0, 0) = \Sigma_{\rho 1}(q_0, 0) + \tilde{\Sigma}_{\rho 1}(q_0, 0) + \Sigma_{\rho 2}(q_0, 0) + \Sigma_{\rho 2}^0 + \Sigma_{\rho 3}(q_0, 0) + \Sigma_{\rho 3}^0 + \Sigma_{\rho 4}(q_0, 0) + \Sigma_{\rho 4}^0 + \Sigma_{\rho 5}(q_0, 0).$$
(B.51)

The imaginary part can be calculated from  $\Sigma_{\rho 1}$ ,  $\tilde{\Sigma}_{\rho 1}$ ,  $\Sigma_{\rho 2}$ ,  $\Sigma_{\rho 3}$ ,  $\Sigma_{\rho 4}$ , and  $\Sigma_{\rho 5}$ , by converting  $\frac{1}{q_0+v-v'+i\epsilon}$  into a delta-function and performing the remaining integrations. The real part can then be calculated through a dispersion relation,

$$\operatorname{Re}\Sigma_{\rho}^{VC}(q) = \frac{-1}{\pi} \operatorname{p.v.} \int_{0}^{\infty} \frac{dv^{2} \operatorname{Im}\Sigma_{\rho}^{VC}(v, \vec{q})}{q_{0}^{2} - v^{2}} + \Sigma_{\rho 2}^{0} + \Sigma_{\rho 3}^{0} + \Sigma_{\rho 4}^{0} , \qquad (B.52)$$

where we do not perform a subtraction, because we have explicitly calculated the nondispersive constant with  $\Sigma_{a2}^0$ ,  $\Sigma_{a3}^0$ , and  $\Sigma_{a4}^0$ .

#### References

- [1] R. Rapp, J. Wambach, Low mass dileptons at the CERN SPS: evidence for chiral restoration?, Eur. Phys. J. A 6 (1999) 415, arXiv:hep-ph/9907502.
- [2] R. Rapp, J. Wambach, H. van Hees, Landolt-Börnstein 23 (2010) 134.
- [3] P. Salabura, J. Stroth, Dilepton radiation from strongly interacting systems, Prog. Part. Nucl. Phys. 120 (2021) 103869, arXiv:2005.14589 [nucl-ex].
- [4] R.-A. Tripolt, F. Geurts, Electromagnetic probes: theory and experiment, Prog. Part. Nucl. Phys. (2022), arXiv: 2210.01622 [hep-ph].
- [5] P. Salabura, HADES, Acta Phys. Pol. B 50 (2019) 1205.
- [6] C. Yang, Q. Yang, STAR, J. Instrum. 15 (07) (2020) C07040.
- [7] Letter of intent for ALICE 3: a next-generation heavy-ion experiment at the LHC, arXiv:2211.02491 [physics.ins-det], 2022.
- [8] M. Greif, C. Greiner, G. Denicol, Phys. Rev. D 93 (2016) 096012.
- [9] S.C. Huot, P. Kovtun, G.D. Moore, A. Starinets, L.G. Yaffe, J. High Energy Phys. 015 (2006).
- [10] D. Fernández-Fraile, A.G. Nicola, Phys. Rev. D 73 (2006) 045025.
- [11] S.I. Finazzo, J. Noronha, Phys. Rev. D 89 (2014) 106008.
- [12] G. Aarts, C. Allton, A. Amato, P. Giudice, S. Hands, J.-I. Skullerud, J. High Energy Phys. 02 (2015) 186.
- [13] B.B. Brandt, A. Francis, H.B. Meyer, H. Wittig, J. High Energy Phys. 03 (2013) 100.
- [14] B.B. Brandt, A. Francis, B. Jäger, H.B. Meyer, Phys. Rev. D 93 (2016) 054510.
- [15] A. Amato, G. Aarts, C. Allton, P. Giudice, S. Hands, J.-I. Skullerud, Phys. Rev. Lett. 111 (2013) 172001.
- [16] G. Kadam, S. Pawar, H. Mishra, J. Phys. G 46 (2019) 015102.
- [17] S. Ghosh, Phys. Rev. D 95 (2017) 036018.
- [18] S. Ghosh, S. Mitra, S. Sarkar, Nucl. Phys. A 969 (2018) 237.
- [19] E.L. Feinberg, Nuovo Cimento A 34 (1976) 391.
- [20] L.D. McLerran, T. Toimela, Phys. Rev. D 31 (1985) 545.
- [21] G. Moore, J. Robert, https://arxiv.org/pdf/hep-ph/0607172.pdf, 2006.
- [22] M. Asakawa, C.M. Ko, Phys. Rev. C 48 (1993) R526.
- [23] B. Friman, H.J. Pirner, Nucl. Phys. A 617 (1997) 496\*\*509.
- [24] G. Chanfray, P. Schuck, Nucl. Phys. A 545 (1992) 271C.
- [25] G. Chanfray, R. Rapp, J. Wambach, Phys. Rev. Lett. 76 (1996) 368.
- [26] M. Urban, M. Buballa, R. Rapp, J. Wambach, Modifications of the rho meson from the virtual pion cloud in hot and dense matter, Nucl. Phys. A 673 (2000) 357, arXiv:nucl-th/9910004.
- [27] R. Rapp, J. Wambach, Thermal properties of a hot pion gas beyond the quasiparticle approximation, Phys. Lett. B 351 (1995) 50, arXiv:nucl-th/9502023.
- [28] C. Song, V. Koch, Phys. Rev. C 54 (1996) 3218.
- [29] M. Herrmann, B. Friman, W. Norenberg, Nucl. Phys. A 560 (1993) 411.
- [30] P.M. Hohler, R. Rapp, Massive Yang–Mills for vector and axial-vector spectral functions at finite temperature, Ann. Phys. 368 (2016) 70, arXiv:1510.00454 [hep-ph].
- [31] J.J. Sakurai, Currents and Mesons, University of Chicago Press, Chicago, IL, 1969.
- [32] M. Urban, M. Buballa, R. Rapp, J. Wambach, Nucl. Phys. A 641 (1998) 433.
- [33] L. Fetter, J.D. Walecka, Quantum Theory of Many-Particle Systems, McGraw-Hill, New York, NY, 1971.
- [34] R. Rapp, Pion-Pion Wechselwirkungen in dichter/heißer Materie, Ph.D. thesis, Institut für Kernphysik Forschungszentrum Jülich, 1996.
- [35] C. Gale, J. Kapusta, Nucl. Phys. B 357 (1991) 65.
- [36] M. Greif, I. Bouras, C. Greiner, Z. Xu, Phys. Rev. D 90 (2014) 094014.
- [37] R. Rapp, J.W. Durso, J. Wambach, Chirally constraining the pi pi interaction in nuclear matter, Nucl. Phys. A 596 (1996) 436, arXiv:nucl-th/9508026.
- [38] C. Froggatt, J. Petersen, Nucl. Phys. B 129 (1977) 89.
- [39] S. Protopopescu, M. Alston-Garnjost, A. Barbaro-Galtieri, S. Flatté, J. Freidman, G. Lynch, M. Rabin, F. Solnitz, Phys. Rev. D 9 (1974) 1872.
- [40] R. Rapp, Pion pion interactions in dense/hot matter, Ph.D. thesis, 1996.

- [41] L. McLerran, Phys. Rev. D 36 (1987) 3291.
- [42] J. Kapusta, Finite Temperature Field Theory, Cambridge University Press, 1989.
- [43] M. Prakash, I. Zahed, Phys. Rev. Lett. 69 (1992) 3282.
- [44] J. Blaizot, E. Iancu, R. Parwani, Phys. Rev. D 52 (1995) 2543.
- [45] M. Prakash, R. Rapp, J. Wambach, İ. Zahed, Isospin fluctuations in QCD and relativistic heavy ion collisions, Phys. Rev. C 65 (2002) 034906, arXiv:hep-ph/0110070.
- [46] P. Gubler, D. Satow, Phys. Rev. D 94 (2016) 094042.
- [47] R. Rapp, G. Chanfray, J. Wambach, Nucl. Phys. A 617 (1997) 472.